General Disclaimer

One or more of the Following Statements may affect this Document

- This document has been reproduced from the best copy furnished by the organizational source. It is being released in the interest of making available as much information as possible.

- This document may contain data, which exceeds the sheet parameters. It was furnished in this condition by the organizational source and is the best copy available.

- This document may contain tone-on-tone or color graphs, charts and/or pictures, which have been reproduced in black and white.

- This document is paginated as submitted by the original source.

- Portions of this document are not fully legible due to the historical nature of some of the material. However, it is the best reproduction available from the original submission.

Multispectral Mapping of the Lunar Surface Using Groundbased Telescopes

Thomas B. McCord*

Carle Pieters*

Michael J. Feierberg

Remote Sensing Laboratory

Department of Earth & Planetary Sciences

24 - 422

Massachusetts Institute of Technology

Cambridge, Mass. 02139

ICARUS

Submitted: November, 1975

Revised: January, 1976

MITRSL Publication #137

*Visiting Astronomers, Cerro Tololo Interamerican Observatory, which is operated by the Association of Universities for Research in Astronomy, Inc., under contract with the National Science Foundation.

26 pages text
1 Table
20 Figures

LUNAR MULTISPECTRAL IMAGING

Thomas B. McCord

22-422

Massachusetts Institute of Technology

Cambridge, Mass. 02139

ABSTRACT

Images of the lunar surface were obtained at several wavelengths using a silicon vidicon imaging system and groundbased telescopes. These images were recorded and processed in digital form so that quantitative information is preserved. The photometric precision of the images is shown to be better than 1%. Ratio images calculated by dividing images obtained at two wavelengths (0.40/0.56μm and 0.95/0.56μm) are presented here for about 50% of the lunar frontside. Spatial resolution is about 2 km at the sub-earth point. A complex of distinct units is evident in the images. Earlier work with the reflectance spectrum of lunar materials indicates that for the most part these units are compositionally distinct. Digital images of this precision are extremely useful to lunar geologists in disentangling the history of the lunar surface.

INTRODUCTION

Sunlight reflected by the surfaces of solar system objects is the dominant source of information available to a remote observer in the spectral region from about 0.3 to 3.0μm. In this spectral region, absorption bands appear in the reflection spectrum of geochemically important solids. Absorptions arise from three different physical processes: (1) molecular vibration, mostly for clathrate solids ("ices") at wavelengths longer than 1μm; (2) electronic transitions of d-shell electrons between orbital states in transition element ions (Fe, Ti, Cr, etc.), in the spectral region 0.5-0.3μm; and (3) charge transfers, due to the exchange of electrons between adjacent ions in the crystal (Fe, Ti, O, etc.), usually at wavelength shorter than 0.8μm.

These absorptions are diagnostic of mineralogy (e.g. Burns 1970;Nash and Conel 1974,Adams 1974,1975).The energies of absorption are controlled by the type of ion or molecule present and the electric field and crystal structure that the ion or molecule experiences at its site in the crystal lattice. These two factors usually define a mineral.

Reflection spectroscopy as a means for remote mineralogical analysis of planetary surfaces has been developed and used mainly for objects other than the earth (cf. Adams and McCord, 1969; McCord et al., 1970; Adams and McCord, 1972; McCord and Gaffey, 1974; see McCord and Adams, 1974; and McCord

et al., 1976 for reviews). Using groundbased telescopes the reflectance spectrum for regions of a surface (Moon, Mars, Mercury, asteroids, satellites, etc.) are measured. These spectra are interpreted using theoretical and laboratory studies of terrestrial, lunar and meteoritic material.

In the case of the moon, the understanding of the surface material optical properties has reached such a level that direct correlation of optical parameters can be made with compositional parameters. For example, the slope of the reflection spectrum between 0.40 and 0.56μm for mature lunar mare soil is directly correlated with TiO_2 content (Charette et al ., 1974) Basaltic mare units can be distinguished based on titanium content. By mapping the spatial distribution of the slope of the reflectance spectrum, a map of titanium content in the mare soil and thus a map of some mare basalt geologic units can be obtained. Other optical and compositional parameters are correlated, but this case illustrates the point.

The differences in color properties which often signify compositional differences in lunar soils are usually small (0.1-10%). The precision of measurement required to map the appropriate optical parameters in two-dimensions has strained the available technology. Recently, a new two-dimensional imaging device has been developed and used by us to obtain improved data.

There have been several earlier attempts to map color differences on the moon. Photographic techniques have been used for more than sixty years (Wood, 1912, 1914; Miethe and Seegert 1911, 1914; Hargreaves, 1924; Wright, 1929; Scott, 1967, personal communication and 1964; Barabashov, 1953; Whitaker, in Kuiper 1966; Whitaker, 1972; Adams 1966, personal communication; see McCord, 1968, for a review). Several impressive maps have been produced, but the photometric inaccuracy and nonlinearity of the photographic process have limited the precision to about 3% at best. Nevertheless, Whitaker's (1972) photographic maps have been used successfully for lunar geologic studies in recent years.

Soderblom (1970) used a point photoelectric photometer and a drift scanning technique to map color in the Mare Serenitatis-Mare Traquillitatis region of the moon. The photometric accuracy of the measurements are probably high (<1%) but the spatial resolution is low (about 30 km). More extensive measurements are now underway (Soderblom, personal communication).

More recently, Johnson, et al, (1975) presented a color map of Mare Serenitatis made using a silicon vidicon imaging system patterened after the system used in this study. Comparison between our data and those of Johnson, et al. for the Mare Serenitatis area shows agreement better than 1% in color difference.

Multispectral maps present here have been used in studies of the lunar surface (Pieters et al. 1974, 1975; Head et al, 1976). The reader is referred to these articles for an example of how color maps are used in lunar geology.

MULTISPECTRAL IMAGING SYSTEM

A two-dimensional imaging system using a silicon diode array vidicon tube was first used at the telescope in 1971 (McCord and Westphal, 1972). Subsequently, the imaging system and observational techniques have been vastly improved. For several years, an advanced design imaging system has been used by our laboratory. Performance tests (McCord and Frankston, 1975; McCord, Frankston and Bosel, 1975) indicate the detector and the imaging system are linear with $\gamma=1.00$ to better than 0.5% over a dynamic range of 3×10^4. The photometric precision is about 0.1% of a full scale signal ($\sim 10^6$ photons) per pixel element. Thus the device is capable of the high precision measurement required in lunar colorimetry.

The data presented here were obtained using a 256 x 250 pixel format on a 1 cm^2 area of silicon vidicon tube (RCA 4532). An area of the moon was imaged through an interference filter onto the detector. A shutter controlled the length of the exposure, which for the moon ranged between several tenths and several tens of seconds. After exposure the image was read out using a raster scanned electron beam to recharge the target discharged by the incident light. The video signal, which is the recharge current, was digitized directly and written onto magnetic tape. The result is an

array of 256 x 250 12 bit integers. Before recording an image, the vidicon target was prepared according to a procedure described by McCord and Frankston (1975). The cycle time for each lunar image is one to two minutes so that hundreds of images were sometimes obtained in one night.

DATA HANDLING

At the telescope the images were viewed in several ways on a monitor (Brookes, 1975) as they were read from the detector or from the recording data tape. However, no permanently stored processing was carried out. The recorded images were calibrated and analyzed in our laboratory using an interactive and a batch image processing system we developed (McCord, Kinnucan and Fawcett, 1975). By working at a CRT terminal, the calibration and analysis processes required to produce geochemical maps were carried out as the results were observed by the operator on the screen.

The standard calibration procedure, to which all raw images were treated, is shown in figure 1. At the telescope, an exposure was made of a uniformly illuminated field. The flat field image was used to calibrate the instrument for sensitivety variations across the field. Also, a dark field image was made by following all procedures for obtaining a lunar image, except the shutter was never opened. Dark field images were later used to calibrate signal offsets and establish a zero signal level. Flat fields were obtained at least once every observing night, by imaging the light scattered from the

inside of the telescope dome. Dark fields were made every 15 to 30 minutes. The calibration process was performed digitally by computer.

A variety of analysis processes were applied to the calibrated images (CI) and the results can be displayed in many ways (McCord, Kinnucan and Fawcett, 1975) Calibrated images were converted to photographs using a CRT film converter. Also, calibrated images of the moon made at several wavelengths were overlayed, registered and divided to produce ratio images. The ratio images were noise filtered and contrast enhanced for display. Enhancement was carried out by calculating the mean intensity value of the ratio image. The ratio image intensity values were then scaled so that the mean value became 1.000, and so that the photograph made of the ratio image would register black for ratio values less than 0.94 and white for ratio values greater than 1.06.

Each image or ratio image (approximately 150 km on a side at the subearth point on the moon) was converted to photographic form and the individual photographs were then mosaicked. The resulting mosaics were copied photographicly

The images can be analyzed by studying the photographic representations presented here. In addition, the CRT interactive terminal can be used by the analyst to further process the image and bring out features of special interest. Alternative forms of hard copy output such as contour plots and intensity profiles can also be obtained. The image is

always available in numerical form so that quantitative studies are possible.

THE LUNAR REFLECTANCE SPECTRUM

The wavelengths at which a surface is imaged must be chosen with great care in order that the color maps bring out geologic and geochemical features and so that the color images can be interpreted in terms of known physical processes affecting the optical properties. Poorly chosen bandpasses lead to a massive data reduction exercise resulting in poor discrimminibility of lunar units.

For the moon, we preceded our imaging program with a study of the reflection spectrum between 0.3 and 1.1μm at many lunar locations. The absorption features were analyzed using theoretical studies and laboratory analysis of lunar surface materials (Adams and McCord, 1970, 1971a,b, 1972, 1973; Adams et al., 1974; Adams,1967, 1974a,b; McCord and Adams, 1973, 1974). Examples of the spectral reflectance for a variety of lunar areas is shown in figure 3. To bring out the subtle differences, all spectra were divided by the reflectance for a standard area in Mare Serenitatis to produce relative reflectance spectra (figure 4). The relative spectra were classified, according to the curve shapes, into a variety of lunar spectral types (McCord, 1969; McCord et al., 1972). These spectral types can be understood in terms of lunar soil properties (Adams and McCord, 1972).

To distinguish between various lunar spectral types we chose to image the moon at the wavelength listed in Table 1. However, we present here only data obtained at three wavelength (0.40, 0.56, 0.95μm). The interference filters have the characteristics given in Table 1 and were specially manufactured to pass high quality images.

DATA ACQUISITION

The lunar images shown here are samples of data acquired in a large ongoing observational program. We have used mainly the 60-inch (140 cm) telescope at Cerro Tololo Interamerican Observatory and the 60-inch (140 cm) telescope at Mt. Wilson Observatory. The observations are difficult to acquire because the telescope must track smoothly in both right ascension and declination and the optics must be extremely clean (low scattering) and well aligned (good image resolution). High quality atmospheric seeing is also required for high resolution images. It is our experience that all these factors are difficult to achi e simultaneously. Nevertheless, data of useful quality have been acquired at least three wavelengths for approximately 50% of the lunar frontside with a spatial resolution of better than about 2 km (see figure 5). This coverage consists of about 500 images.

PHOTOMETRIC ACCURACY

Although the performance of the imaging systems was tested by other means (McCord and Frankston, 1975; McCord, et al., 1975) we compared the lunar image data with spectra

obtained using photomultiplier detectors and identical filters. Two lunar areas (a and b) about 10 km in diameter, for which reflectance spectra R(λ) have been measured using photoelectric techniques (McCord et al., 1972), were chosen within one vidicon image. A relative reflectance spectrum (RR) was calculated from both the photoelectric data and the vidicon image using the lunar area b as a standard.

$$RR\ (\lambda) = \frac{R_a(\lambda)}{R_b(\lambda)} \Big/ \frac{R_a(5.6\mu m)}{R_b\ (.56\mu m)}$$

Figure 6 shows relative spectra obtained for the same areas using both techniques. The agreement between these independent techniques for this lunar area as well as at other areas checked is usually within 1%.

Since most lunar regions were imaged only at three wavelengths (0.40, 0.56, 0.95μm), a comparison between photoelectric and vidicon measurements is possible only at these wavelengths for many areas. Figure 7 shows the correlation between 0.40/0.56μm and 0.95/0.56μm reflectance ratios obtained by both methods of measurement for about 10 km diameter lunar areas. The correlation is within about 1%. Random atmospheric extinction variations usually occur at this level of precision even on "clear" nights.

DATA PRESENTATION

Mosaics of all useful lunar vidicon images obtained and processed as of October 1975 are shown in figures 8, 9,

and 10. Figure 8 images were obtained at 0.56μm and are similar to what would be seen by the eye with some contrast enhancement. Figure 9 is a mosaic of the 0.40/0.56μm ratio images processed as depicted in figure 2. Figure 10 has undergone the same process using the 0.95/0.56μm ratio.

Figures 9 and 10 are multispectral maps in which brightness changes represent differences in the reflectance of lunar areas at one wavelength relative to that at another. In figure 9 brighter means relatively bluer, or higher reflectance at 0.40μm relative to 0.56μm. In figure 10 brighter means redder, or higher reflectance at 0.95μm relative to 0.56μm.

Both ratio images were drastically contrast enhanced (the ratio range from black to white is 0.94-1.06) to bring out the small differences in reflectance. Variations of 1% in color differences are easily seen in these images. As shown in the previous section, the images are photometrically precise to at least this level. The contrast enhancement chosen for these ratios we found to give the best overall visibility for the color boundaries present. However, the photographic representations of the digital images do not show all the information present. Changing the contrast brings out additional features. In several of our projects designed to apply these data to lunar geologic problem, we found it necessary to work with several contrast versions.

The spatial resolution of 2 km or less obtained in most of these images is not displayed in the full moon mosaics shown in figures 8 - 10. Therefore, sections of this mosaic are presented at expanded scale in figures 11 - 16.

PROBLEMS

These mosaics of lunar images are the result of a first attempt at calibrations and analysis. Individual images were not matched so that a shade of gray in one image may not represent the same color difference as the same shade of gray in another image. Each ratio image has been contrast enhanced by the same amount but the choice of reflectance ratio to be designated unity varies. Geometric fidelity is not maintained across the mosaics. The images were acquired at difference lunar librations and through several different telescopes; no attempt has been made to place the images on a standard projection.

In addition the user should be aware of the existence of defects in some of the images resulting from a slight mismatch between the two frames divided to make a ratio. This results in "false shadows" appearing at sharp contrast boundaries and can be due to a processing error or to changes in atmospheric seeing during the observation. Other problems, such as noise associated with a scan line (due to electrical interference) are obvious in some images and create artificial affects.

We have repeatedly imaged several areas to check consistency and find the ratio image reporduced even in the very fine detailed to ~1% so that with the cautions raised above, the geologist should be able to use the data with confidence.

SIGNIFICANCE

The significance of the color difference displayed in the ratio images or mutlispectral maps has been partially worked out using laboratory and theoretical studies of the optical properties of lunar materials, as is discussed earlier in this paper. Although it is not the purpose of this paper to discuss lunar geology, it is useful for the reader to understand some of the implications of the spectral features.

For example, the 0.95/0.56μm ratio image shows variations in brightness which are correlated with craters. Fresh craters appear darker, i.e. they are more absorbing at 0.95μm relative to 0.56μm than are the surrounding regions. This occurs partly because an electronic transition absorption band appears in the reflectance spectra near 0.95μm especially for fresh lunar material, due to the mineral pyroxene (Adams and McCord, 1970) and partly because charge transfer absorptions appear strongest in the spectra at shorter wavelengths especially for weathered lunar material, due to the creation of agglutinitic materials (Adams and McCord, 1973; Adams and Charette, 1975). Due to weathering, fresher soil contains more crystalyn pyroxene and mature soil contains more agglutinitic material and thus fresher soil has a stronger electronic transition absorption band and more mature soil has a stronger charge transfer absorption. So the 0.95/0.56μm ratio image maps soil maturity. More subtle differences also occur in the 0.95/0.56μm ratio images which are a measure of the composition of the pyroxene minerals. As

the absorption band shifts away from the wavelengths passed by the interference filter used to obtain the 0.95μm image, the degree of absorption measured in the ratio image will decrease.

Another example of the significance of the multispectral images concerns the 0.40/0.56μm ratio image and the areas of Mare Serenitatis near the Apollo 17 landing site. Figure 17 shows the 0.40/0.56μm ratio image for this area next to a 0.56μm image. Three prominent mare units are evident in the ratio image.

As was discussed earlier in this article Charette, et al., (1974) presented a relationship between TiO_2 content of mature mare soil and the slope of the reflectance spectrum between 0.40 and 0.56μm. Using that relationship and the photometrically precise ratio image in figure 17, a contour map of TiO_2 content can be calculated for this Mare Serenitatis area (figure 18).

POLARIZATION MAPS

In carrying out this program, one of us (CP) attempted to map the degree of polarization of reflected radiation using the same equipment and techniques. The results of one attempt are shown in figure 19. This lunar area at the entrance to Mare Humorum (lat. 17°S, long. 35°W) was imaged (at phase angle 88°) through an interference filter centered at 0.56μm. A polarizing filter was also placed in the optical path so that it transmitted light, first in the plane of the

reflection, and then in a perpendicular plane. The same exposure time was used for each image. After calibration as depicted in figure 1, the digital images were processed so as to calculate polarization for each pixel (i,j) in the classical manner.

$$P_{ij} = \left(\frac{I_{\perp} - I_{\parallel}}{I_{\perp} + I_{\parallel\, ij}}\right)$$

Figure 19 is a photographic representation of the polarization map in which brighter indicates higher polarization. The contrast enhancement is from 2% (for black) to 14% (for white) polarization. The dependence of polarization on albedo, well known from other measurements, is obvious. The uniformity of polarization within the mare is striking.

The precision of this technique for mapping polarization can be estimated using figure 20. Here is shown the distribution of polarization calculated for each pixel of a flat field. The flat fields were made with the polarizing filter oriented in two perpendicular directions and polarization was calculated as in the case of the lunar image.

FUTURE PLANS

Observations of the unmapped portion of the lunar front side are continuing. Existing and future maps will be placed on a standard lunar grid to correct geometric distortions. The individual images will be photometrically adjusted to eliminate frame-to-frame variations in contrast. A standard data base should result which can be used by lunar scientists.

Even with the large amount of data presented or to be obtained in this program, much new work will remain. The spatial resolution of the groundbased images can only be improved to 1 km at best because of the effects of the earth's atmosphere. The backside of the moon is inaccessible from the earth. From the surface of the earth several important spectral regions, where compositional information exists, are unusable because of atmospheric absorption. All of these limitations are removed if an instrument could be orbited about the moon.

As mentioned earlier, the basic compositional information is contained in the full reflectance spectrum. Thus, ideally, one requires maps of the moon at many wavelengths (about 300) in order to have the full spectrum for all lunar areas. Again, a long-lived lunar orbiting spacecraft experiment could provide such data. Projects such as the one reported here hopefully are precursors of such spacecraft experiements.

ACKNOWLEDGEMENTS

We thank the Hale Observatories and the Cerro Tololo Interamerican Observatory for making available most of the telescope time used to obtain the images presented here. This research is supported by NASA Grant NGR 22-009-730. The instrument development was partially supported by NSF Grant GP 31516. This is publication number 137 of the Remote Sensing Laboratory.

REFERENCES

Adams, J.B. (1974b). Visible and near infrared diffuse reflectance spectra of pyroxenes as applied to remote sensing of solid objects in the solar system. J. Geophys. Res. 79, 4329-4836.

Adams, J.B. (1975). Uniqueness of visible and near-infrared diffuse reflectance spectra of pyroxenes and other rock-forming minerals. In Infrared and Raman Spectroscopy of Lunar and Terrestrial Minerals. (C. Karr, Jr., Ed), pp. 91-xxx. Academic Press, New York.

Adams, J.B. and Charette, M.P. (1975). Effects of maturation on the reflectance of the lunar regolith: Apollo 16--a case study. The Moon. 13, 293-299.

Adams, J.B. and Filice, A.L. (1967). Spectral reflectance 0.4 to 2.0 microns of silicate rock powders. J. Geophys. Res. 72, 5705-5715.

Adams, J.B. and McCord, T.B. (1969). Mars: interpretation of spectral reflectivity of light and dark regions. J. Geophys. Res. 74, 4851-4856.

Adams, J.B. and McCord, T.B. (1970). Remote sensing of lunar surface mineralogy: Implications from visible and near-infrared reflectivity of Apollo 11 samples. In Proc. of Apollo 11 Lunar Sci. Conf. (A.A. Levinson, Ed.), pp. 1937-1945. Pergamon Press, New York.

Adams, J.B. and McCord, T.B. (1971a). Alteration of lunar optical properties: Age and composition effects. Science. 171, 567-571.

Adams, J.B. and McCord, T.B. (1971b). Optical properties of mineral separates, glass and anorthistic fragments from Apollo mare samples. In Proc. of 2nd Lunar Sci. Conf. (A.A. Levinson, Ed.), pp.2183-2195. MIT Press, Cambridge.

Adams, J.B. and McCord, T.B. (1972). Electronic spectra of pyroxene and interpretation of telescopic reflectivity curves of the moon. In Proc. of 3rd Lunar Sci. Conf. (D.R. Criswell, Ed.), pp.3021-3034. MIT Press, Cambridge.

Adams, J.B. and McCord, T.B. (1973). Vitrification darkening in the lunar highlands and identification of descartes material at the Apollo 16 site. In Proc. of 4th Lunar Conf. (W.A. Gose, Ed.), pp.163-177. Pargamon Press, New York.

Adams, J.B., Pieters, C. and McCord, T.B. (1974). Orange glass: Evidence for regional deposits of pyroclastic origin on the moon. In Proc. of 5th Lunar Sci. Conf. (W.A. Gose, Ed), pp. 171-187. Pargamon Press, New York.

Barabashov, N.P. (1935). On color contrasts of the lunar surface. Circ. Kharkov Astr. Obs. 12, 3.

Brooks, M. (1975). A digital solid state scan converter with unusual display capabilities. Applied Optics.14, 1835-1838.

Burns, R.G. (1970) In Mineralogical Applications of Crystal-Field Theory. pp. 1-224, Cambreidge University Press, London.

Charette, M.P., McCord, T.B., Pieters, C. and Adams, J.B. (1974). Application of remote spectral reflectance measurements to lunar geology classification and determination of titanium content of lunar soils. J. Geophys. Res. 79, 1605-1613.

Hargreaves, F.J. (1924). An attempt to determine the color of the lunar surface by direct color photography. J. British Astr. Assoc. 34, 243-245.

Head, J., Pieters, C., McCord, T.B., Adams, J.B., and Zisk, S. (1976). Definition and detailed characterization of lunar surface units using remote observations, in preparation.

Johnson, T.V., Matson, D.L., Phillips, R.J. and Saunders, R.S. (1975). Vidison spectral imaging; Color enhancement and digital maps. In Proc. of 6th Lunar Sci. Conf. (R.B. Merril, Ed.), pp. 2677-2688. Pergamon Press, New York.

Kuiper, G.P. (1966). Interpretation of Ranger VII records. Communication no. 58, Lunar and Planetary Lab. of Univ. of Arizona. 4, 18-20.

McCord, T.B. (1968). Color differences of the lunar surface. Ph.D dissertation, Calif. Inst. of Technol., Pasadena, Calif.

McCord, T.B. (1969). Color differences on the lunar surface. J. Geophys. Res. 74, 4395-4401.

McCord, T.B., Adams, J.B. and Johnson, T.B. (1970). Asteroid Vesta: Spectral reflectivity and compositional implications. Science.168, 1445-1447.

McCord, T.B., Adams, J.B. and Huguenin, R.H. (1976). Reflection spectroscopy: An experiment for remotely sensing surface mineralogy and composition. To appear in a NASA-SP (Orbital Science).

McCord, T.B., Charette, M., Johnson, T.V., Lebofsky, L.A., Pieters, C. and Adams, J.B. (1972). Lunar spectral types. J. Geophys. Res. 77, 1349-1359.

McCord, T.B. and Frankston, M. (1975). Observational experience with silicon diode array vidicon at the telescope. Applied Optics. 14, 1437-1446.

McCord, T.B. and Adams, J.B. (1974). The use of groundbased telescope in determining the composition of the surfaces of solar system objects. In Proc. of the Soviet-American Conf. on the Cosmochemistry of the Moon and Planets held in Moscow, USSR, June 4-8. Lunar Science Institute, Houston.

McCord, T.B., Frandston, M. and Bosel, J. (1975). Performance of the MIT silicon vidicon imaging system at the telescope. In Image Processing Techniques in Astronomy (C. de Jager and H. Nieuwenhuijzen, Eds), pp. 91-96. D. Reidel, Boston.

McCord, T.B. and Gaffey, M.J. (1974). Asteroids: Surface composition using reflection spectroscopy. Science. 186, 352-355.

McCord, T.B., Kinnucan, P. and Facett, G. (1975). Image processing systems developed at MIT to handle silicon vidicon imaging and spectra of astronomical objects. In Image Processing Techniques in Astronomy (C. de Jager and H. Nieuwenhuijzer, Eds.), pp. 229-334. D. Reidel, Boston.

McCord, T.B., and Westphal, J.A. (1972). A two-dimensional silicon vidicon astronomical photometer. Applied Optics. 11, 522-526.

Miethe, A. and Seegert, B. (1911). On qualitative differences of light reflected by various parts of the lunar surface. Astron. Nachr. 188, 9,239,371.

Miethe, A. and Seegert, B. (1914). Qualitative differences in the light reflected from various parts of the moon. Astron. Nachr. 198, 4736.

Nash, D.B. and Conel, J.E. (1974). Spectral reflectance systematics for mixtures of powdered hypersthene, labradorite, and ilmenite. J. Geophys. Res. 79, 1615-1621.

Pieters, C., Head, J., McCord, T.B., Adams, J.B., and Zisk, S. (1975). Geological and geochemical units of Mare Humorum: Further definition using remote sensing and lunar sample information. In Proc. of 6th Lunar Sci. Conf. (R.B. Merrill, Ed), pp. 2689-2710. Pergamon Press, New York.

Pieters, C., McCord, T.B., Charette, M., and Adams, J.B. (1974). Dark mantling material in the Apollo 17 soil samples. Science. 183, 1191-1194.

Scott, N.W. (1964). Color on the moon. Nature. 204, 1075-1076.

Soderblom, L.A. (1970). The distribution and ages of regional lithologies in the lunar maria. Ph.D. dissertation, Calif. Inst. of Tech., Pasadena, Calif.

Whitaker, E.A. (1972). Lunar color boundaries and their relationship to topographic features: A preliminary survey. The Moon. 4, 348-355.

Wood, R.W. (1912). Selective absorption of light on the moon's surface and lunar petrography. Ap. J. 36, 74-84.

Wood, R.W. (1914). Petrography of the moon. J. British Astr. Assoc. 24, 370.

Wright, W.H. (1929). The moon as photographed by light of different colors. Pub. Astron. Soc. Pacific. 41, 125-132.

TABLE 1

λe(μm)	Δλ (Fωhp) (Å)	Peak Transmission %
0.353	218	22
0.403	204	51
0.568	235	54
0.735	279	69
0.969	306	67
1.066	327	39

Characteristics of the interference filters used in this study.

FIGURE CAPTIONS

Figure 1. Procedure followed for all object images (OI) to produce photometricly calibrated images (CI).

Figure 2. Sequence of operations performed on calibrated images (CI) of the same lunar region to produce multispectral ratio images (RI).

Figure 3. Spectral reflectance of a variety of lunar areas is shown for the wavelength region of interest here. The wavelength position of the filter through which the images presented here were made are marked.

Figure 4. Relative reflectance spectra for a variety of lunar areas are shown. The reflectance spectra for all areas were divided by the spectra for a standard area in Mare Serenitatis (MS2) to produce relative spectra (McCord et al., 1972). For example, curves MT1 and MS2 in figure 3 were divided to produce curve (MT1/MS2) in this figure. Note the scale enhancement. Subtle differences between the spectra are brought out by this ratio technique.

Figure 5. A lunar frontside map showing the lunar regions for which useful vidicon image data now exist. Additional data should be available soon.

Figure 6. Relative reflectance spectra obtained using a photometric filter photometer (X) are compared with spectra obtained using the vidicon images (•). The two lunar areas used have coordinates 21°N 29°E (Spot 1)

and 21°N 26°E (Spot 2) and are approximately 10 km in diameter. The agreement is within 1%.

Figure 7. Correlation between 0.40/0.56μm and 0.95/.56μm reflectance ratios obtained for the same 16 lunar areas using both photoelelectric and vidicon techniques. Again the agreement is within 1%.

Figure 8. A mosaic of vidicon images of the moon made through an interference filter centered at 0.56μm.

Figure 9. A mosaic of contrast enhanced multispectral images made by numerically dividing images made at 0.40μm by 0.56μm images, according to figure 2. Approximately the same area is covered as in figure 8.

Figure 10. Same as figure 9 except the wavelengths are 0.95μm and 0.56μm.

Figures 11-16. These images are sections of the mosaic of images shown in figures 8-10 but shown at higher resolution to exhibit more of the detail present in the data. Still more information exists at greater resolution. The (a) figures are like figure 8, (b) like 9 and (c) like 10.

Figure 17. The 0.56μm image of southeastern Mare Serenitatis is shown next to the 0.40/0.56μm ratio image. Three major mare basalt units are evident in the color ratio image.

Figure 18. A contour map of the TiO_2 content of the mare basalt units located in a section of the region shown in figure 17.

Figure 19. An image showing percent polarization scaled from 2 to 14 percent (upper right), the same image scaled from 8 to 14 percent (lower left), an independent image scaled from 2 to 14 percent (lower right) and a conventional albedo image (upper left). This area of moon is just north of the Mare Humorum entrance.

Figure 20. The frequency distribution of polarization values obtained for each pixel when the calculation for figure 19 is performed on a flat field where no polarization should exist.

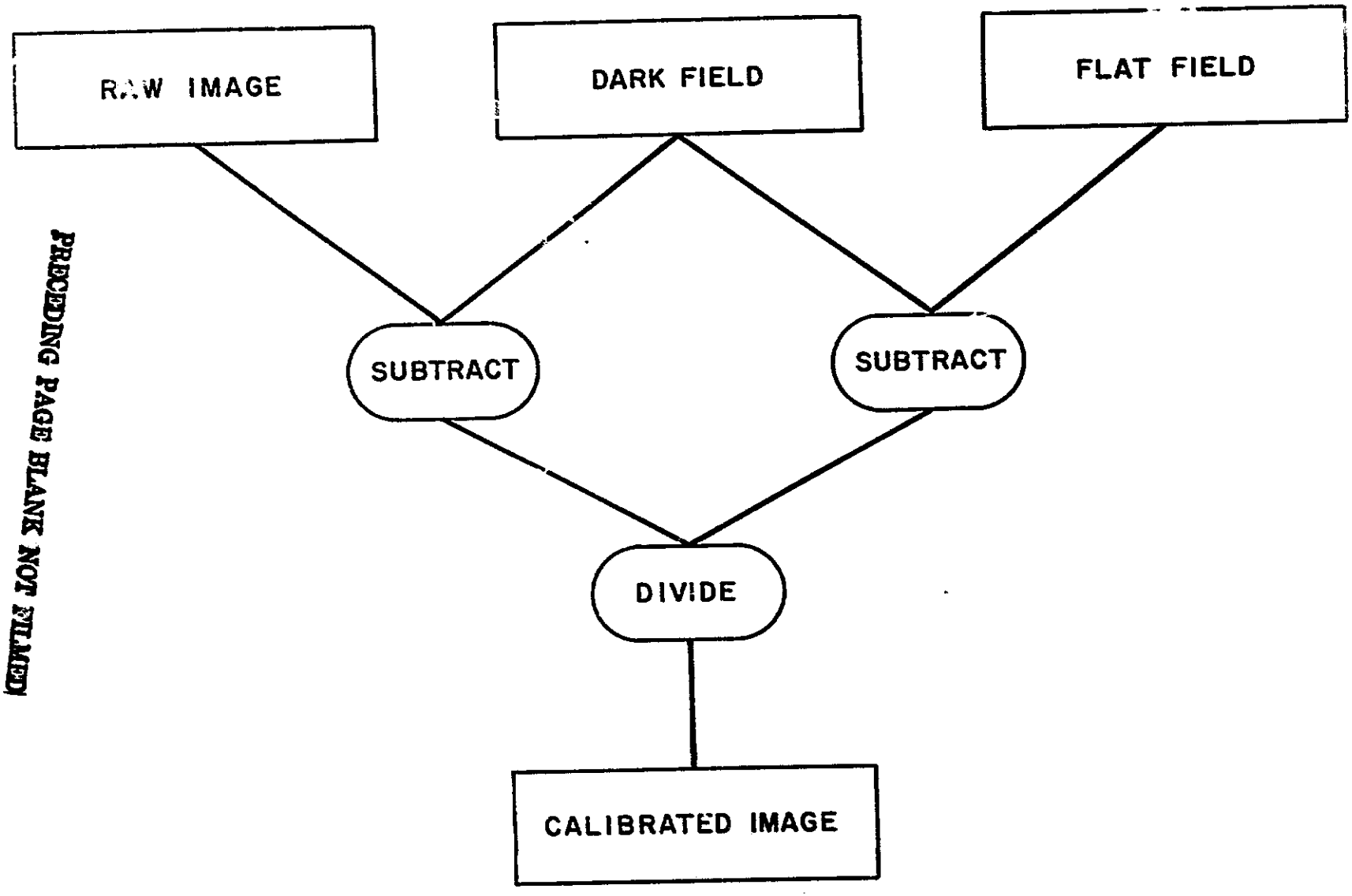

Figure .

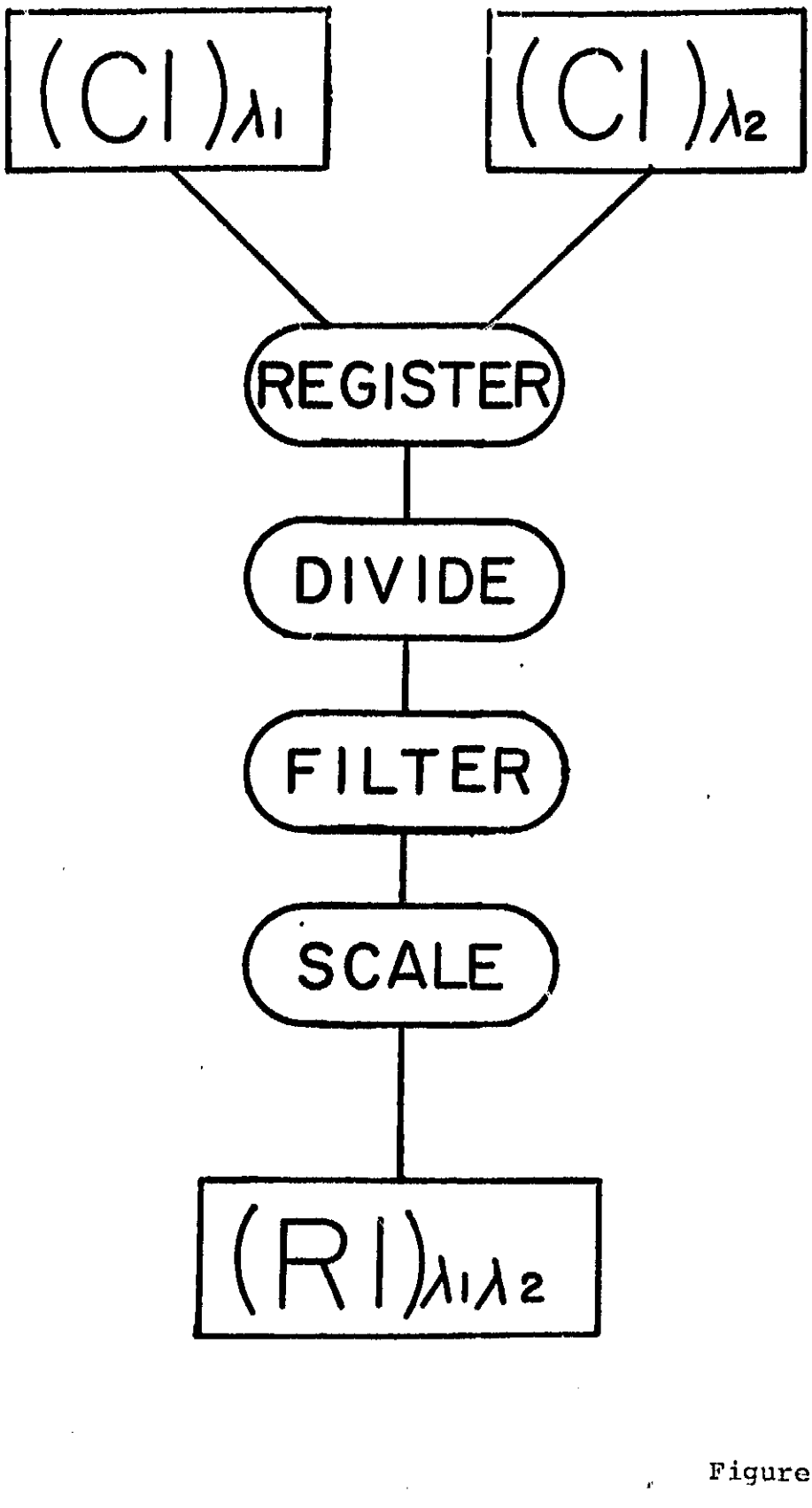

Figure 2

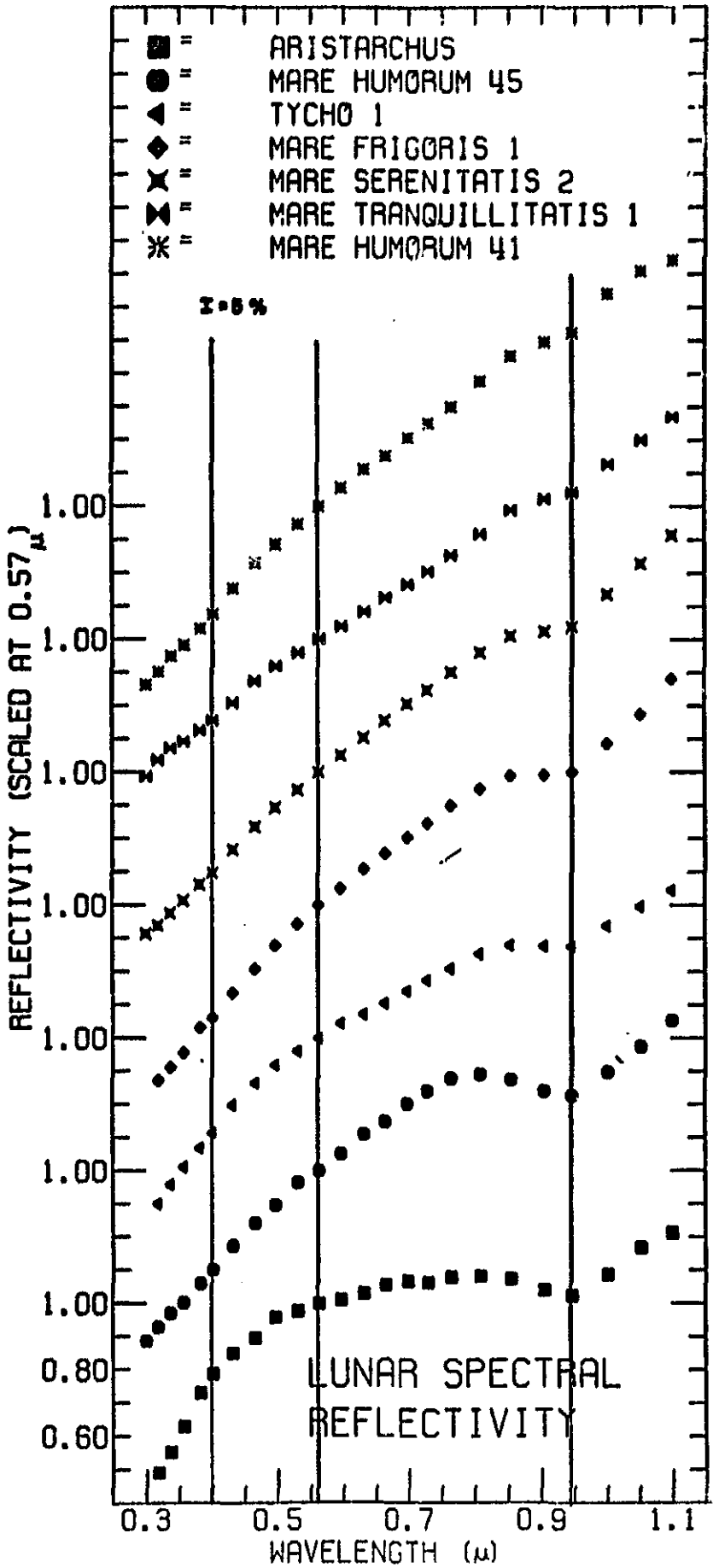
ARISTARCHUS
MARE HUMORUM 45
TYCHO 1
MARE FRIGORIS 1
MARE SERENITATIS 2
MARE TRANQUILLITATIS 1
MARE HUMORUM 41
I=5%
REFLECTIVITY (SCALED AT 0.57μ)
1.00
1.00
1.00
1.00
1.00
1.00
0.80
0.60
LUNAR SPECTRAL
REFLECTIVITY
0.3
0.5
0.7
0.9
1.1
WAVELENGTH (μ)

Figure 3

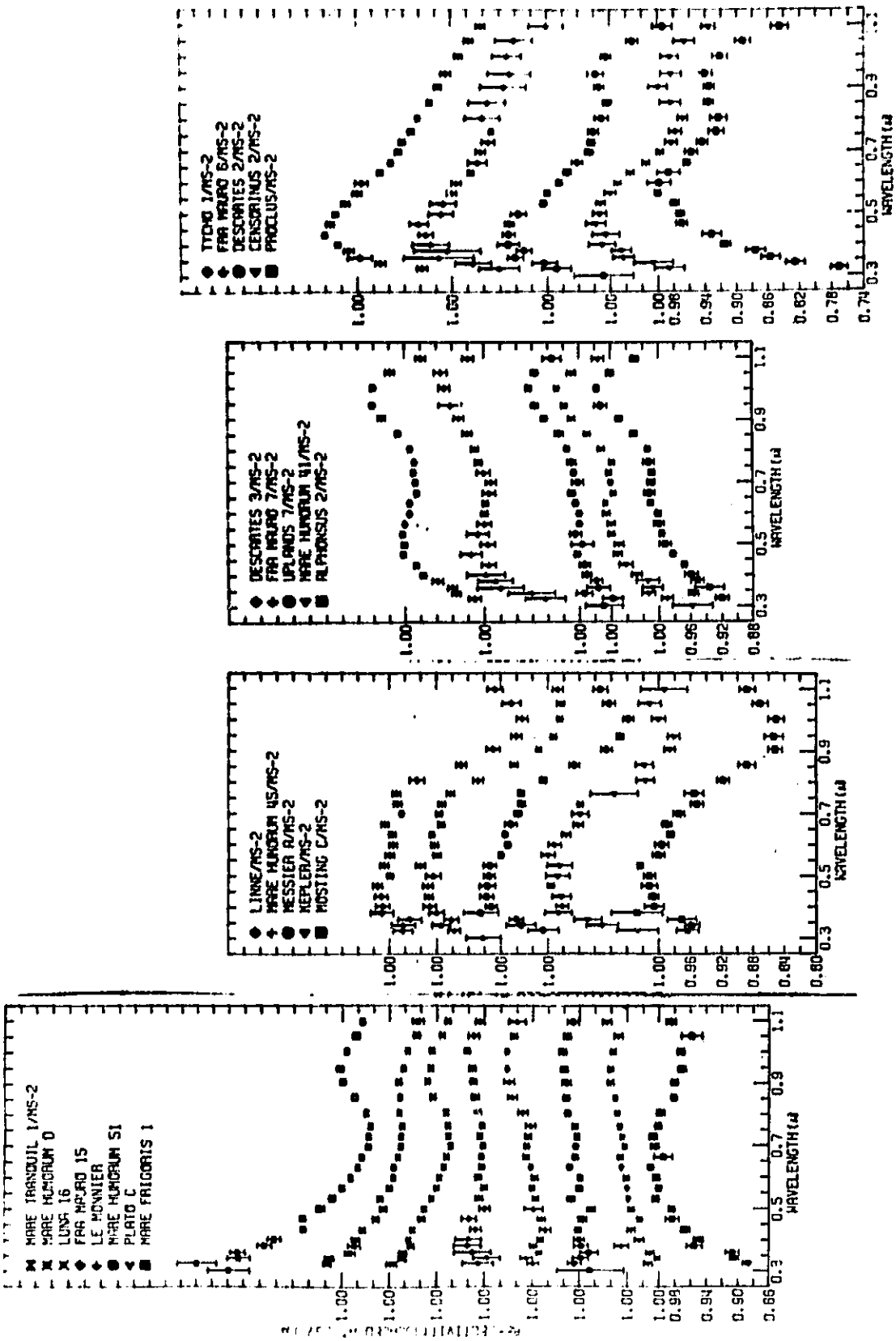

Figure 4

ORIGINAL PAGE IS
OF POOR QUALITY

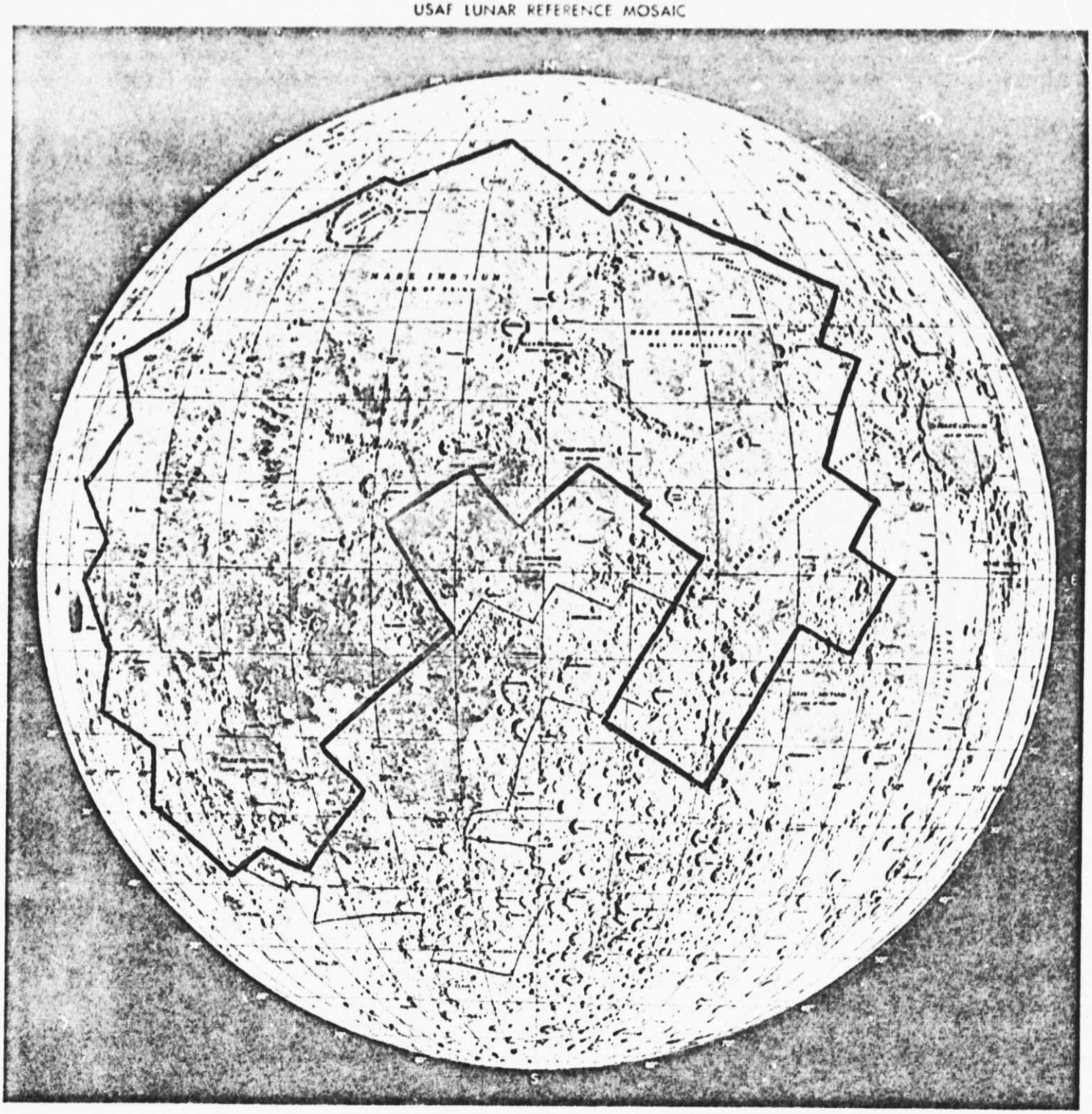

Figure 5

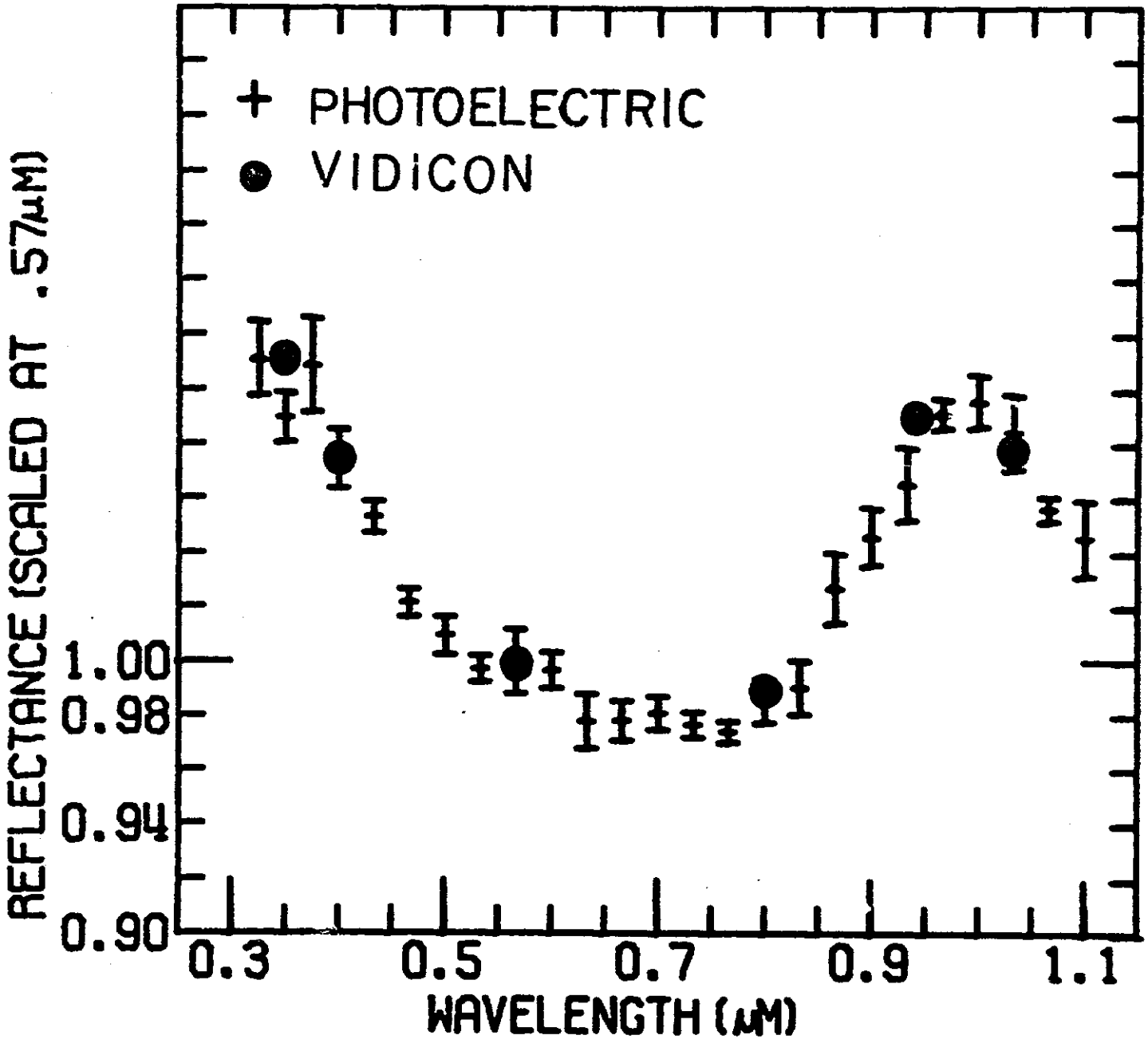
+ PHOTOELECTRIC
● VIDICON
REFLECTANCE (SCALED AT .57μM)
1.00
0.98
0.94
0.90
0.3
0.5
0.7
0.9
1.1
WAVELENGTH (μM)

Figure 6

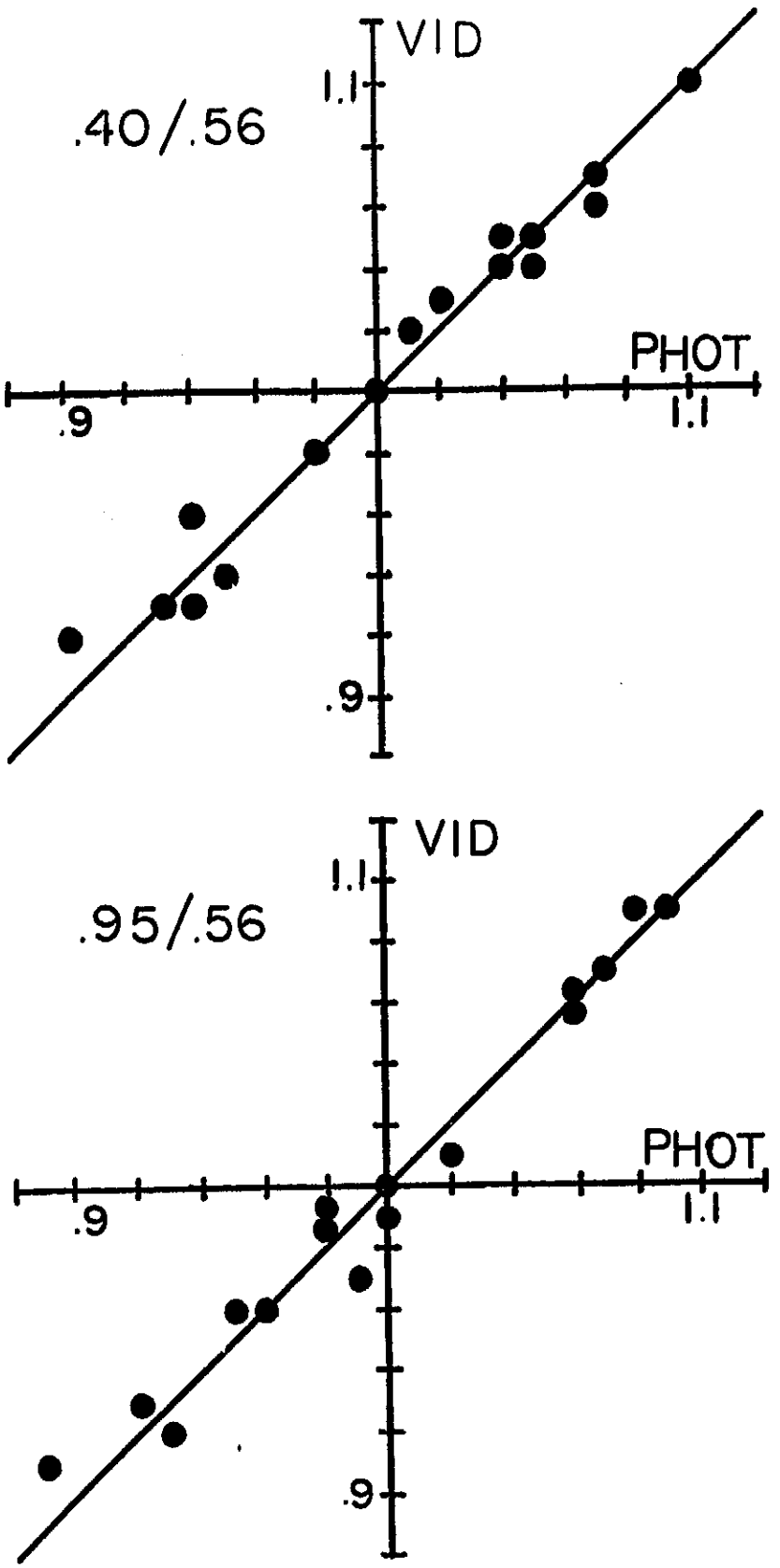

Figure 7

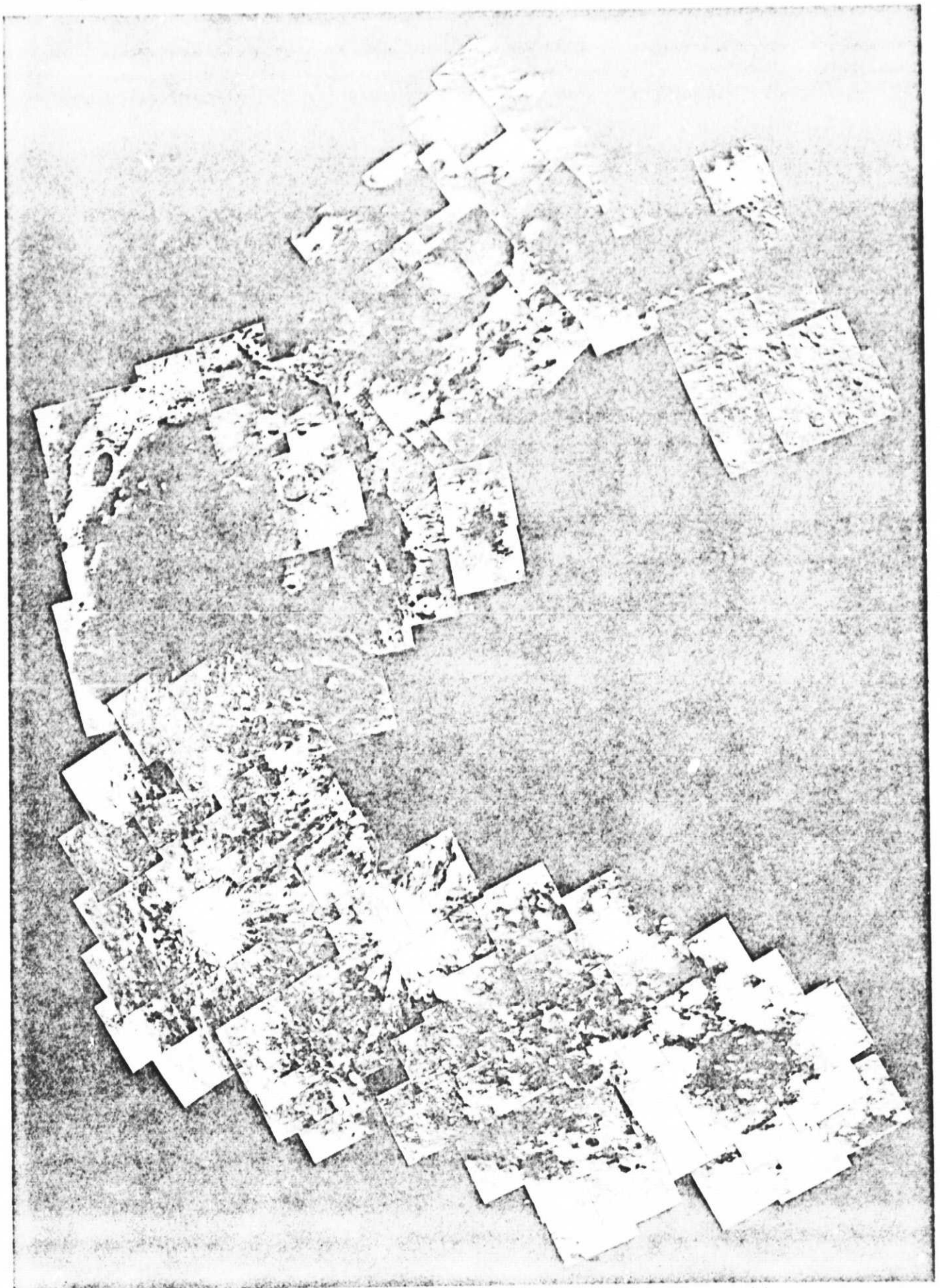

Figure 8

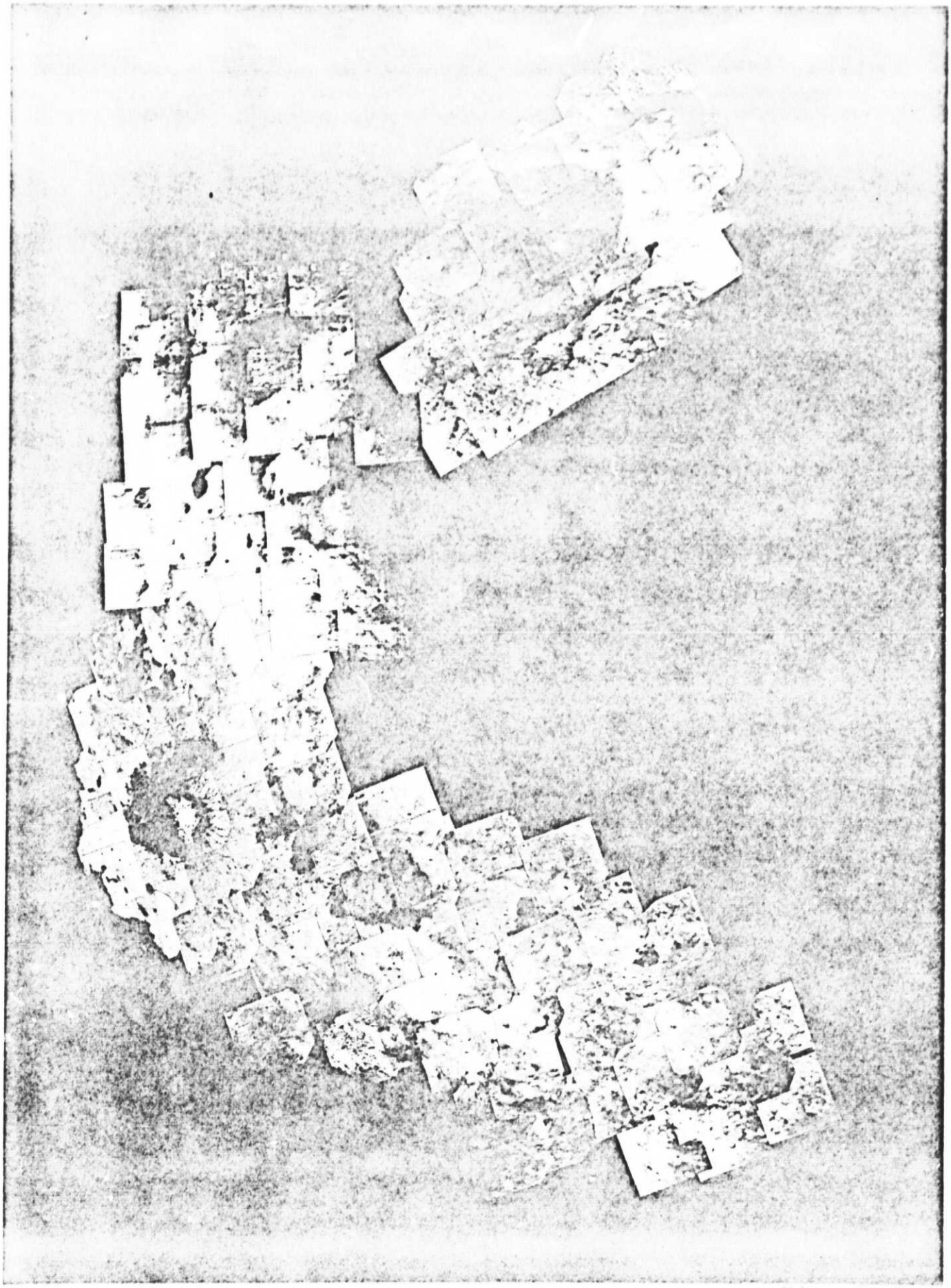

Figure 9

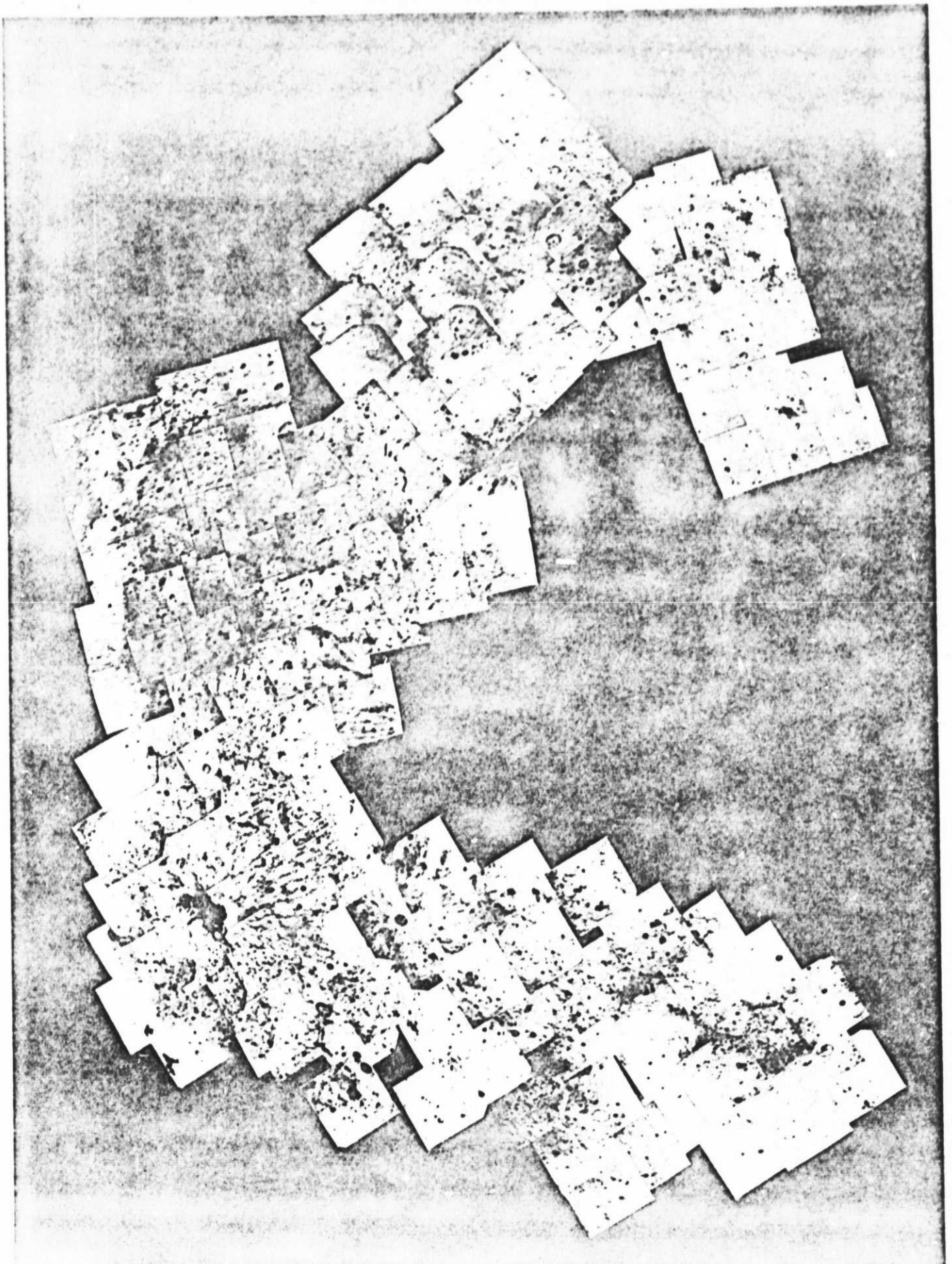

ORIGINAL PAGE IS
OF POOR QUALITY

Figure 10

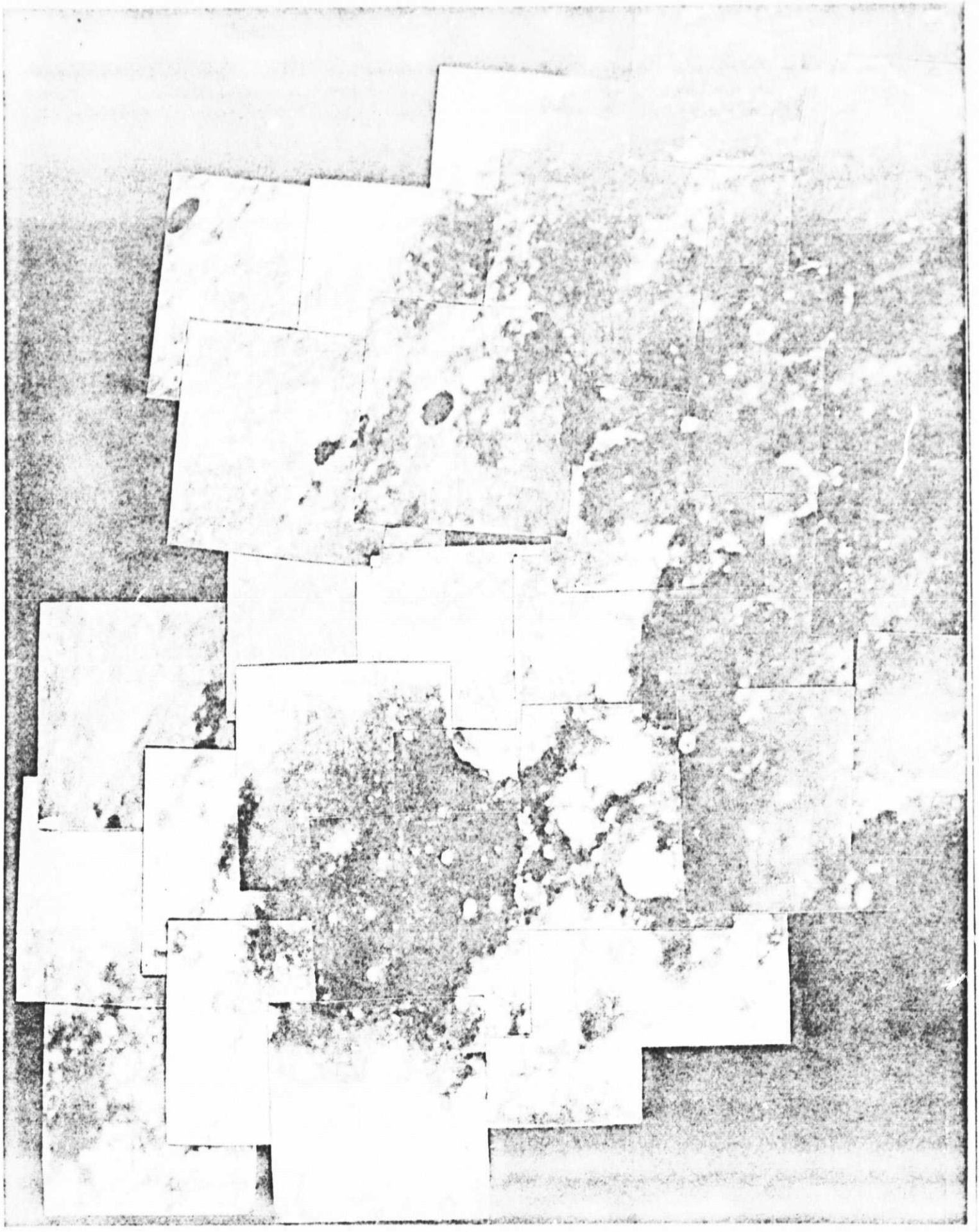

Figure 11b

Figure 11c

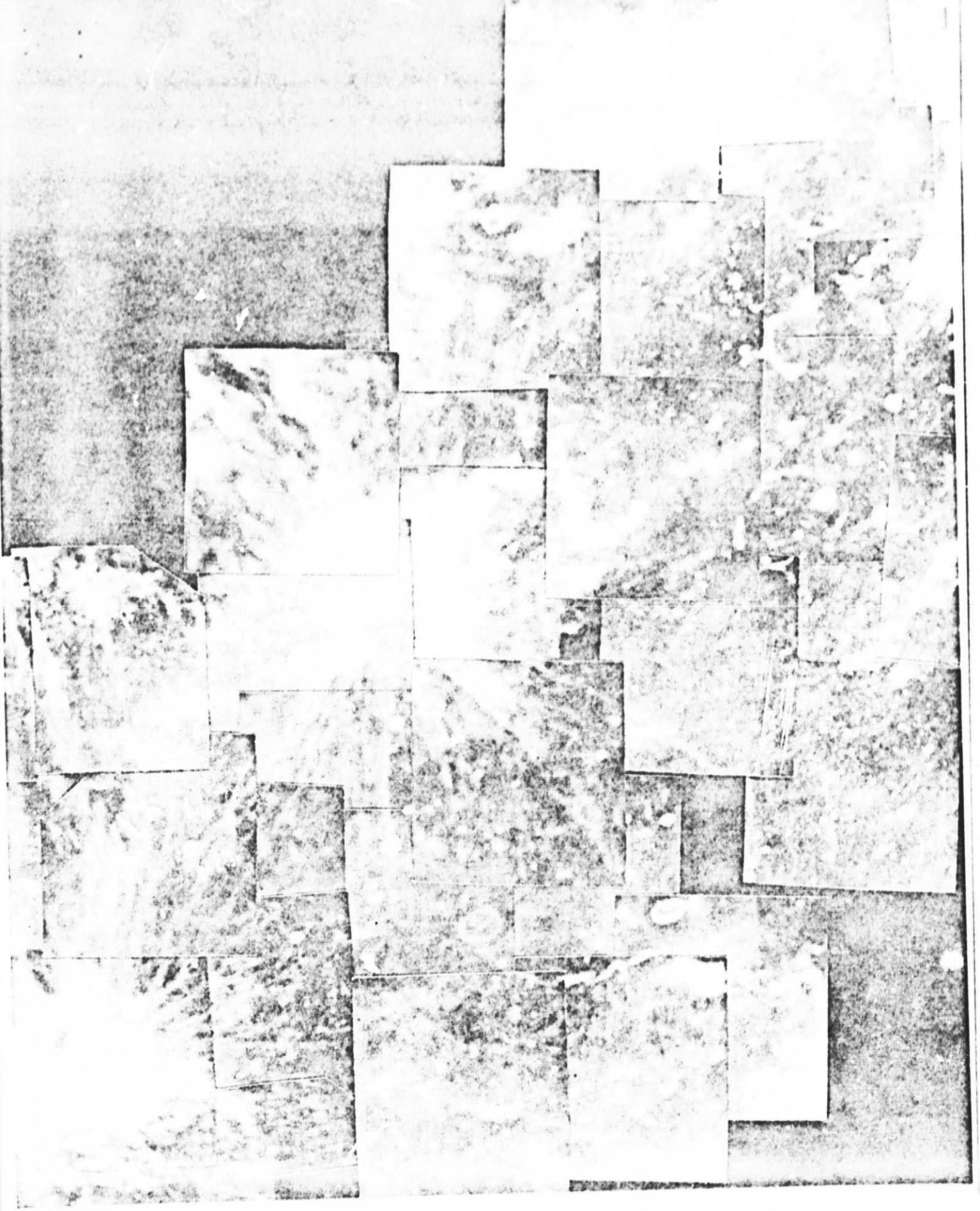

Figure 12b

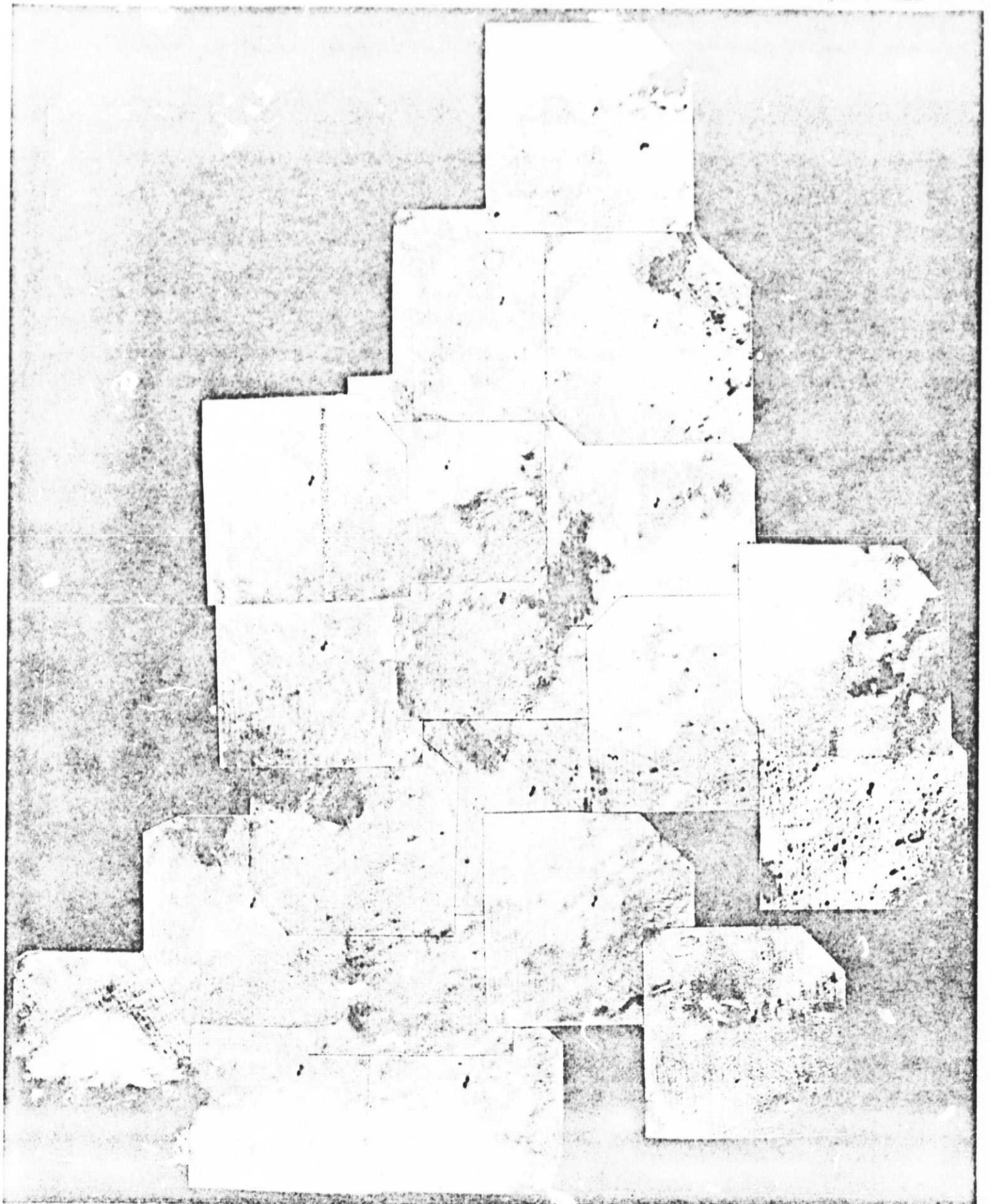

Figure 12c

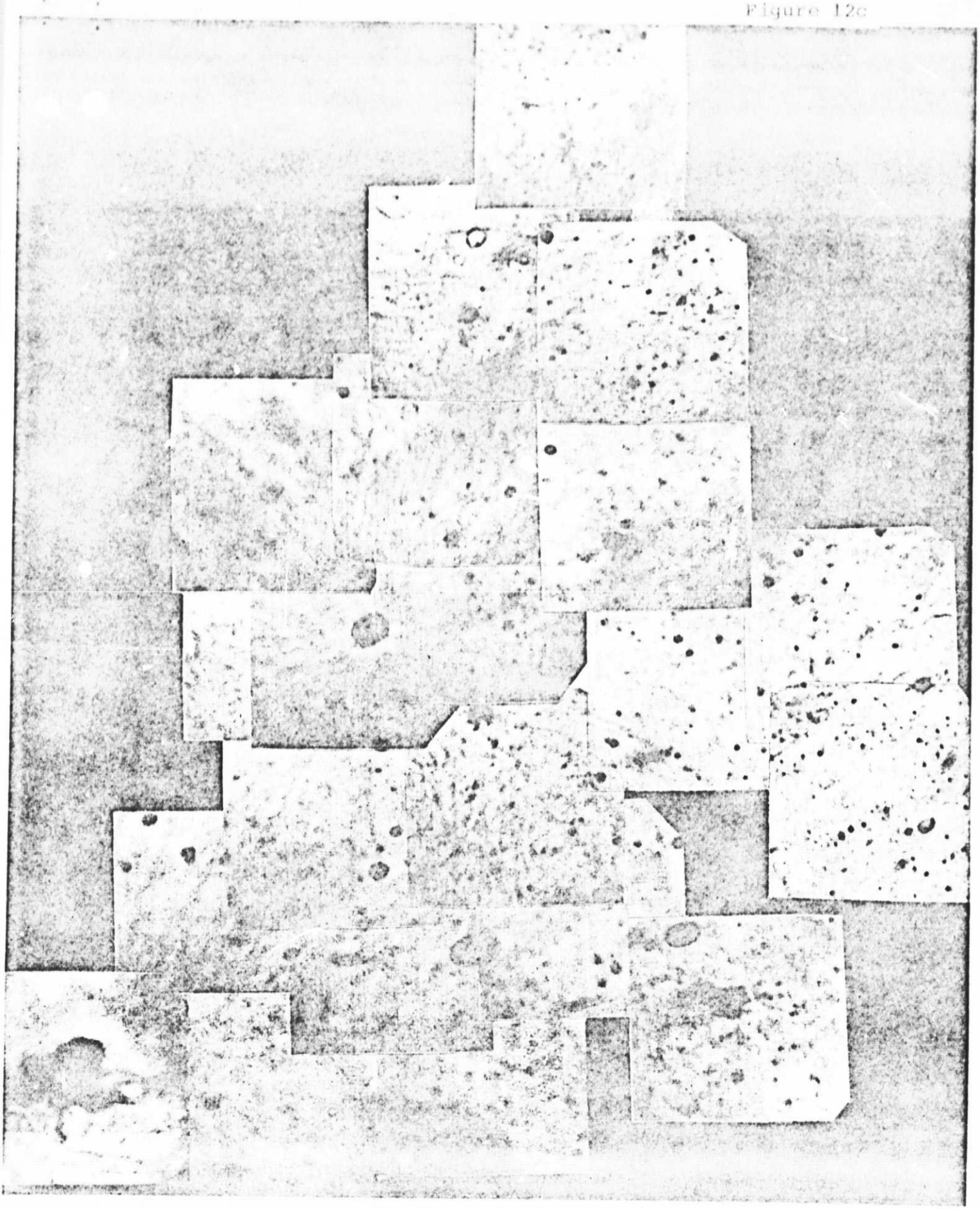

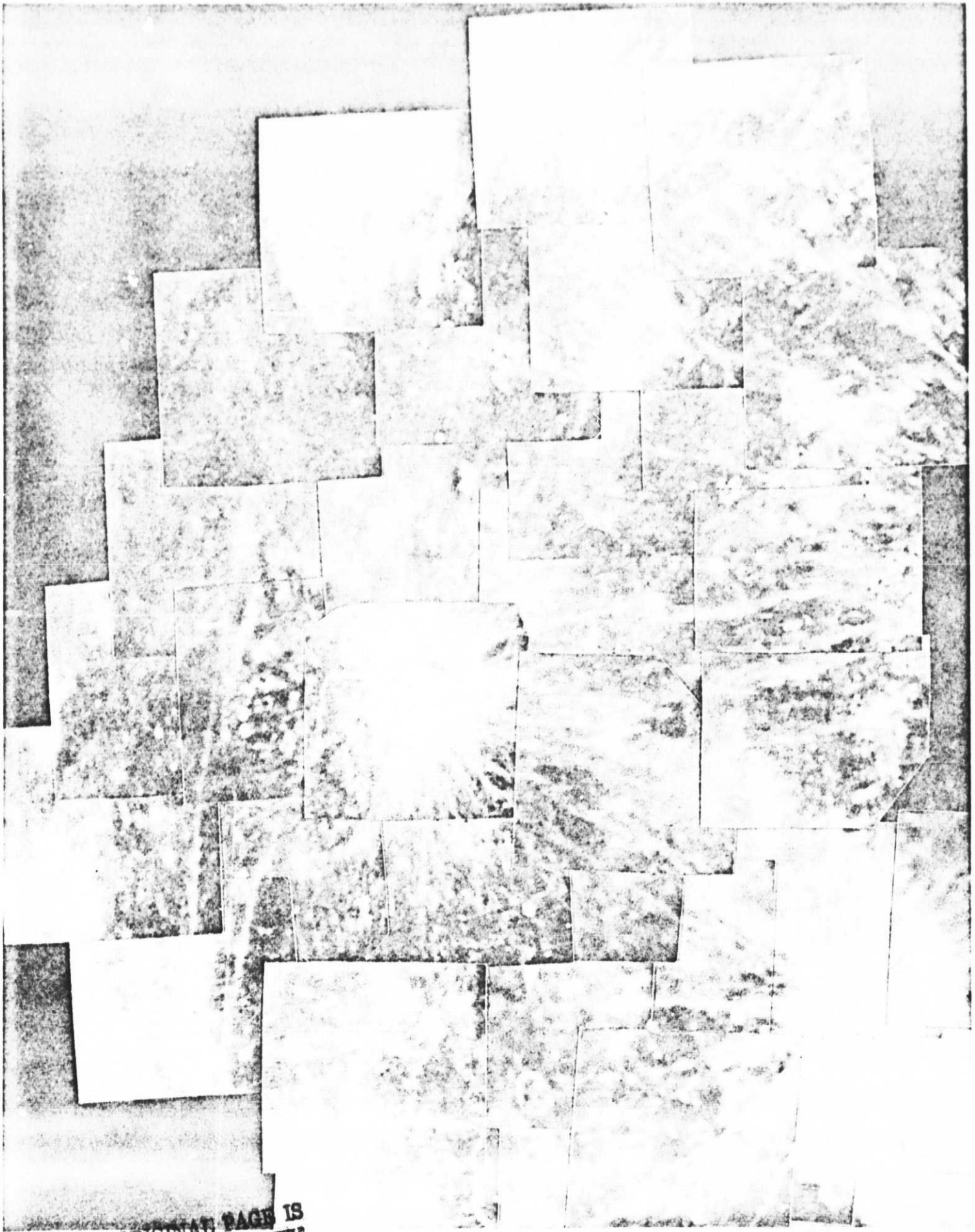

Figure 13a

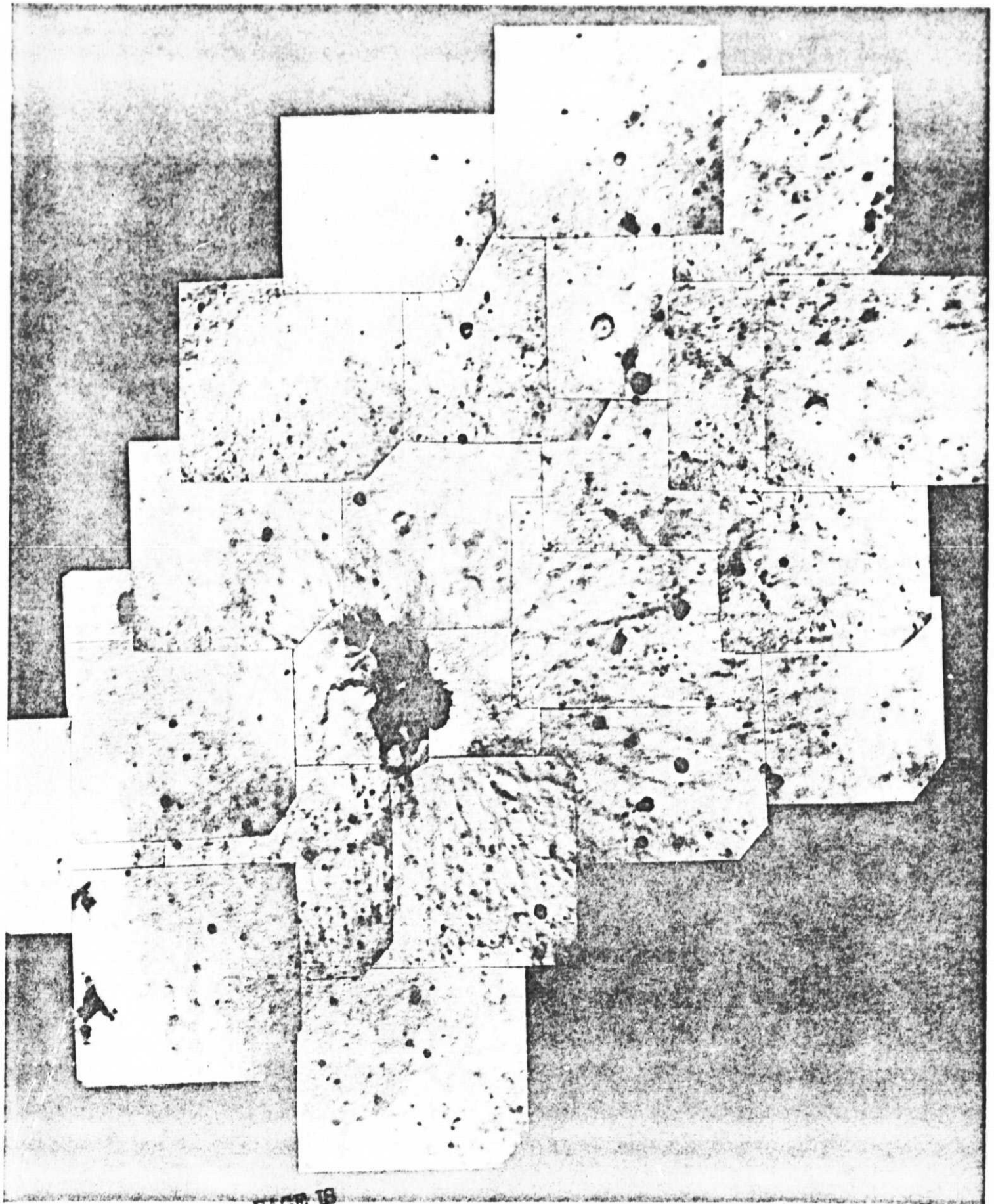

Figure 13c

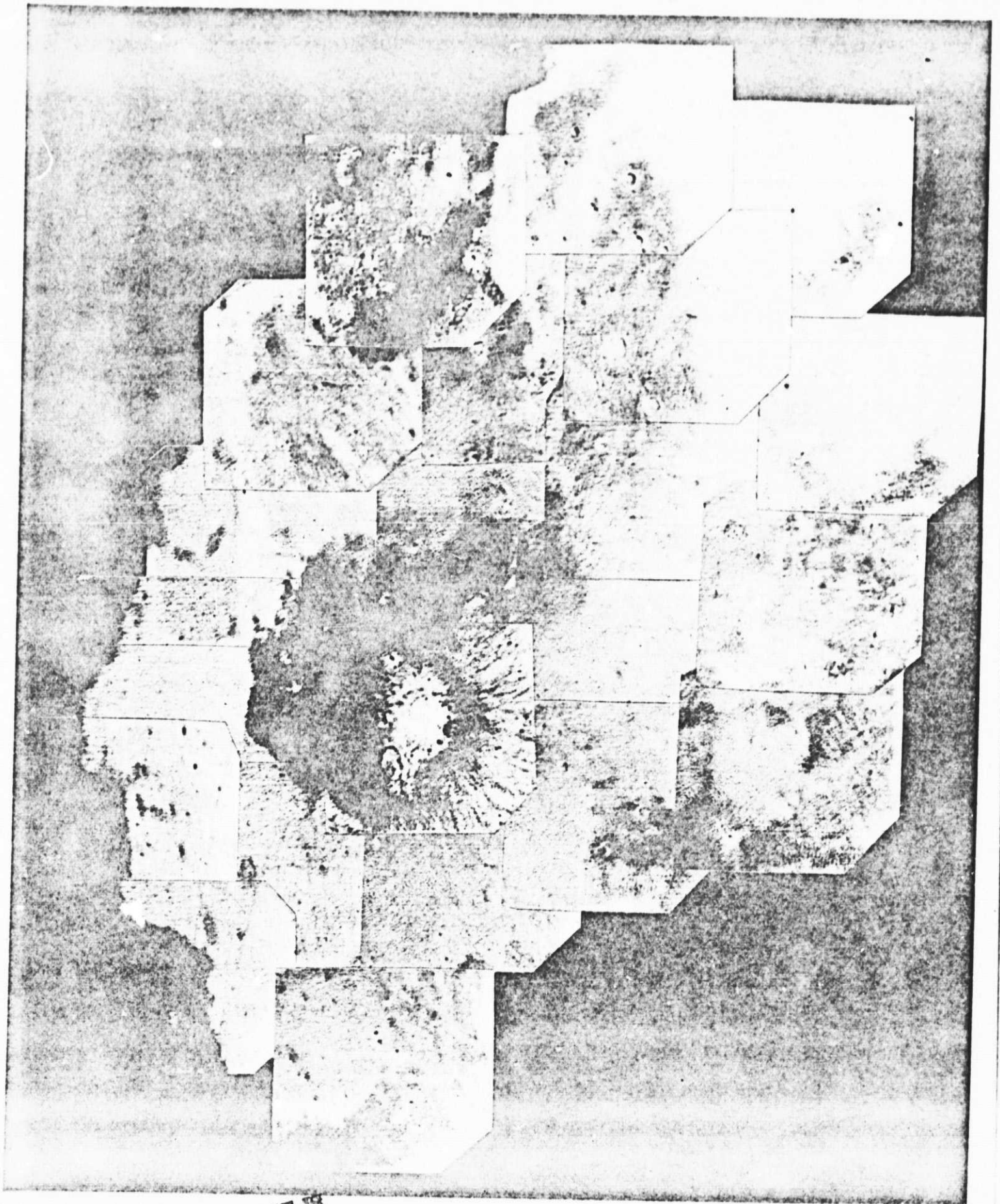

Figure 13b

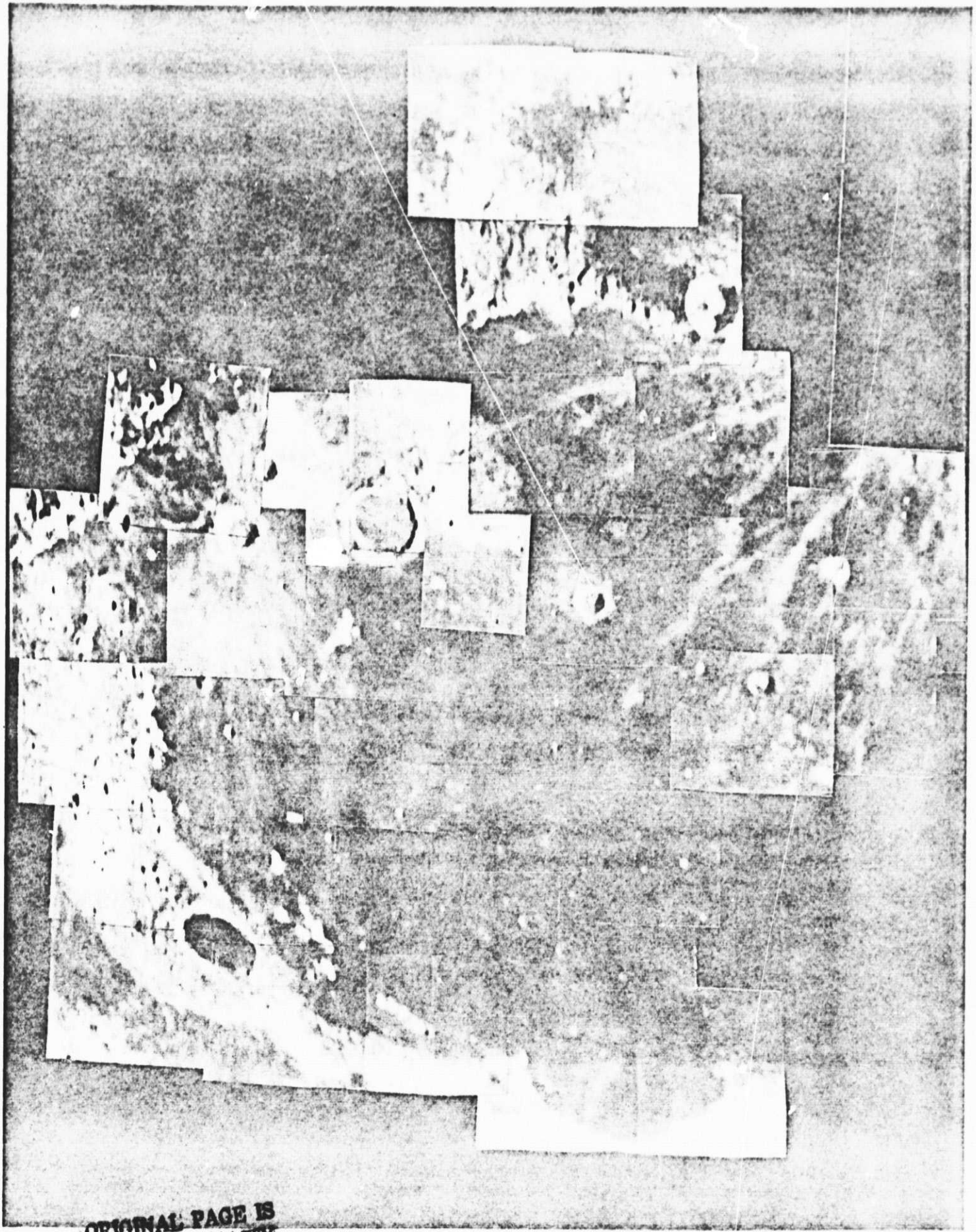

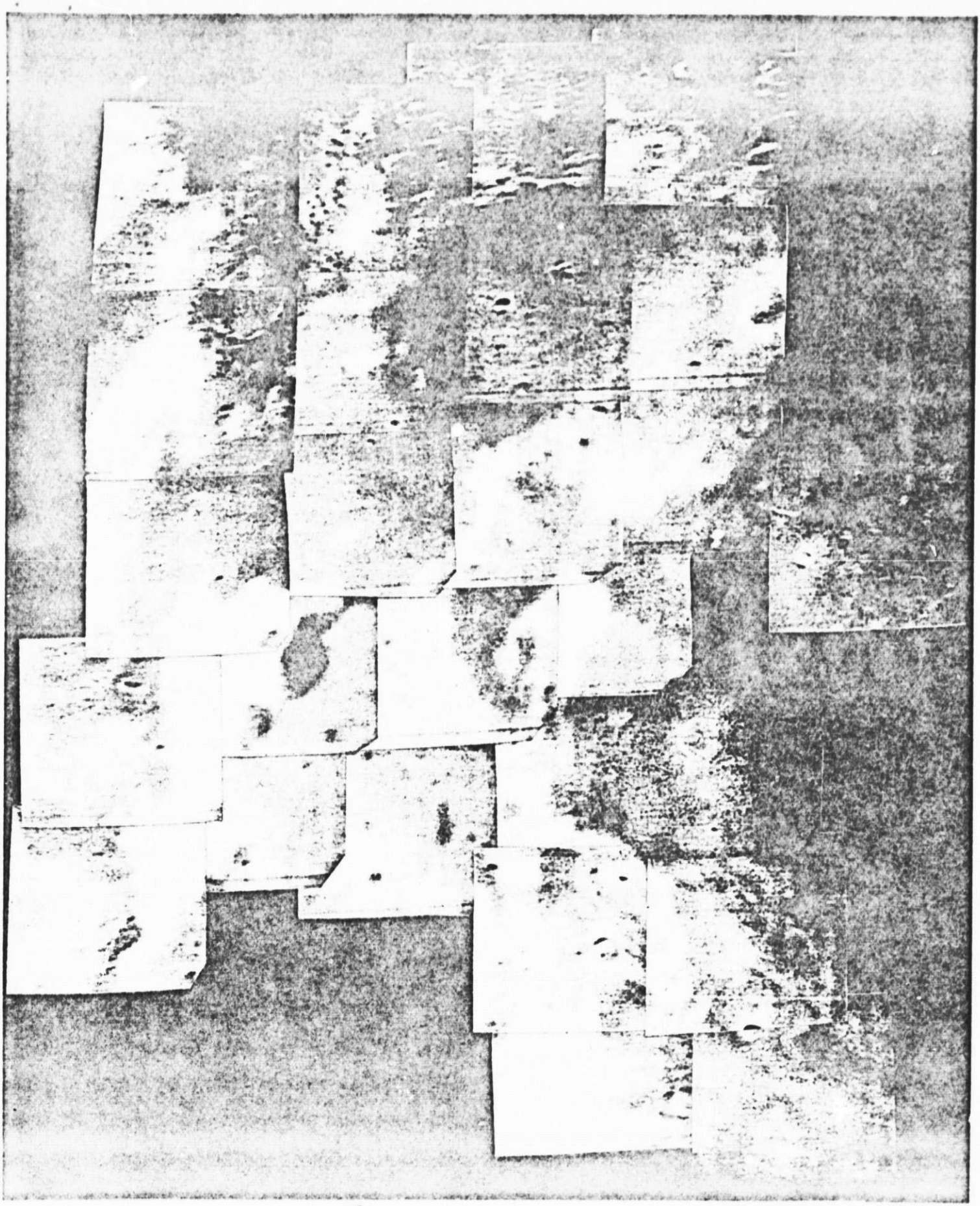

Figure 14b

Figure 14c

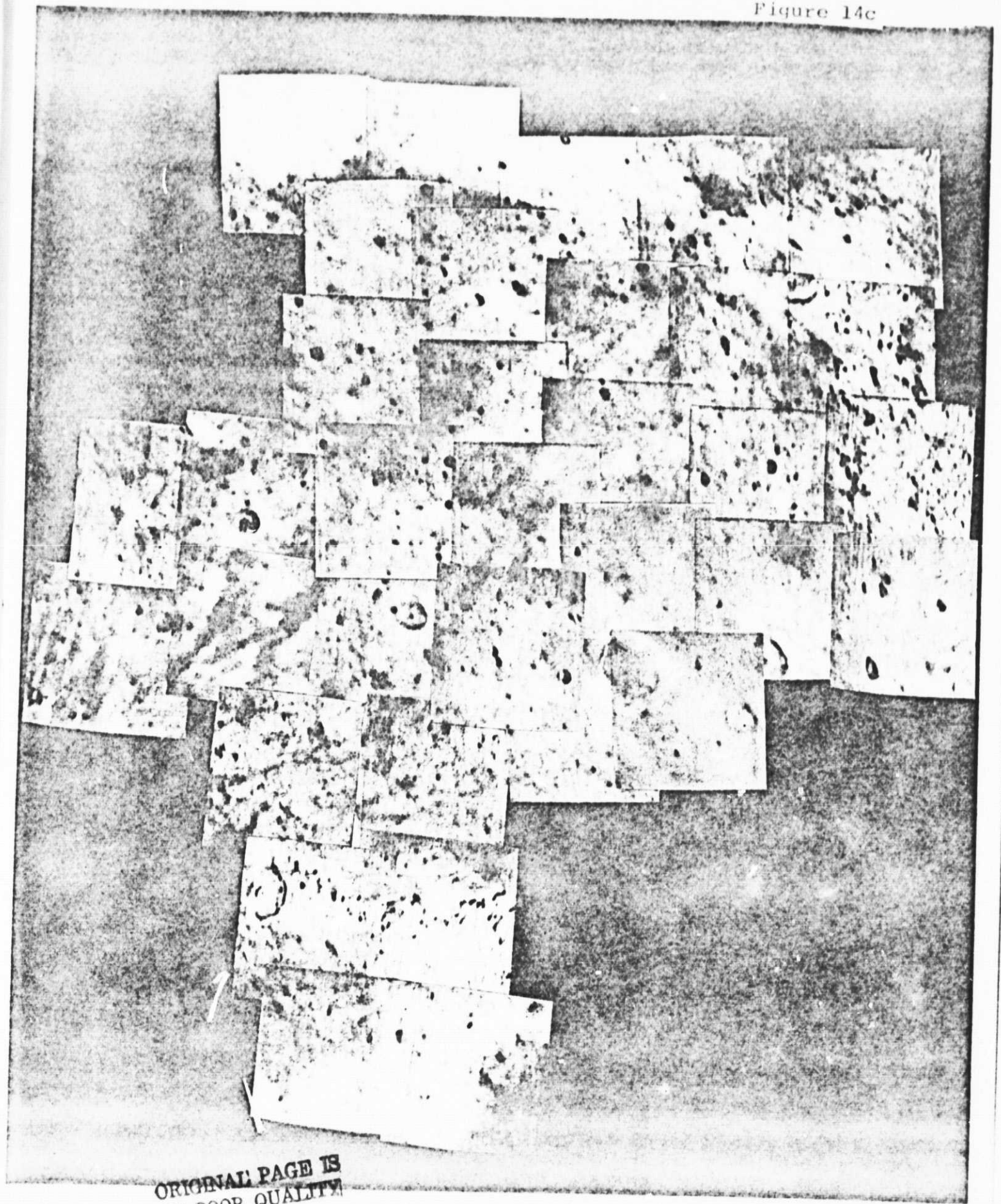

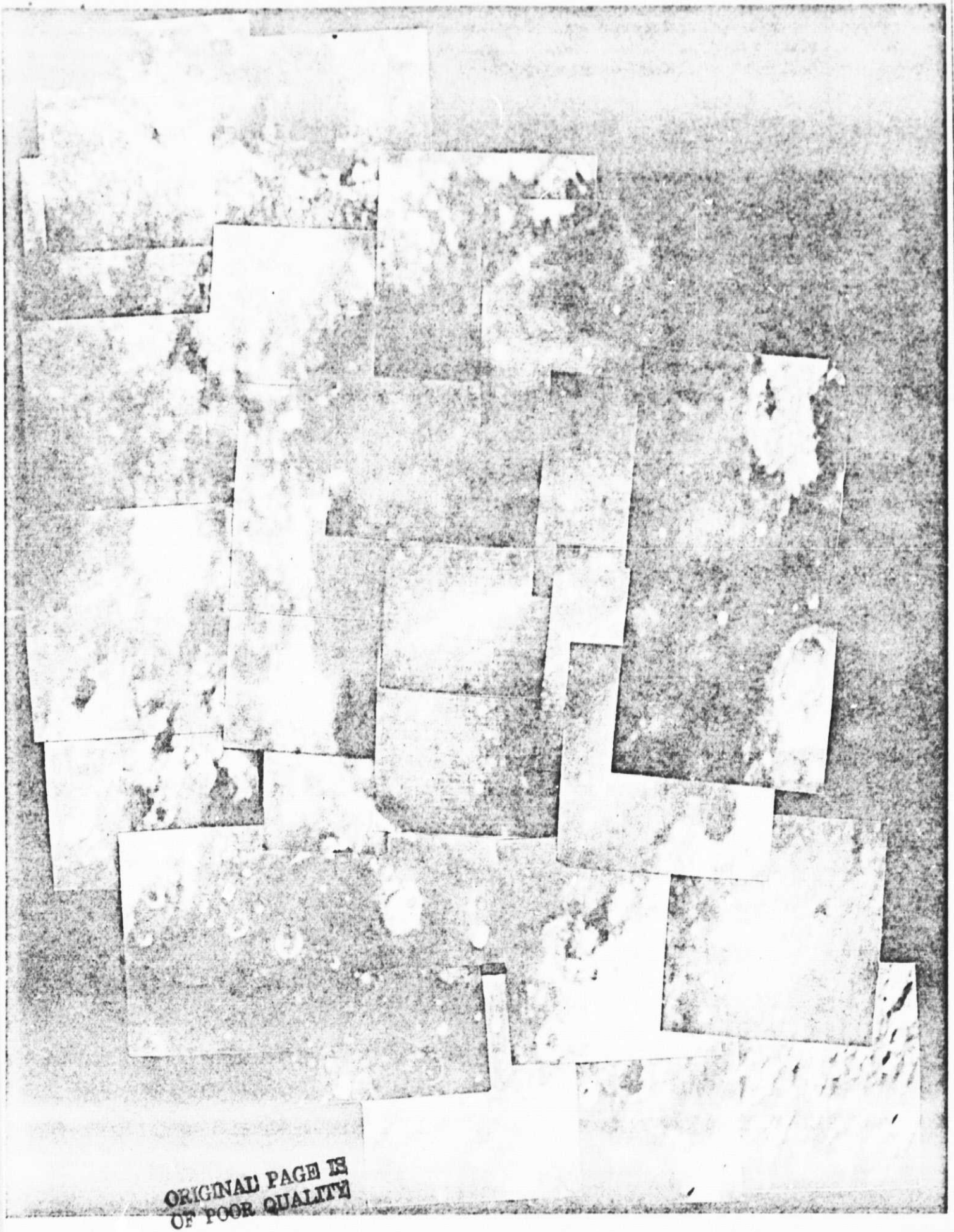

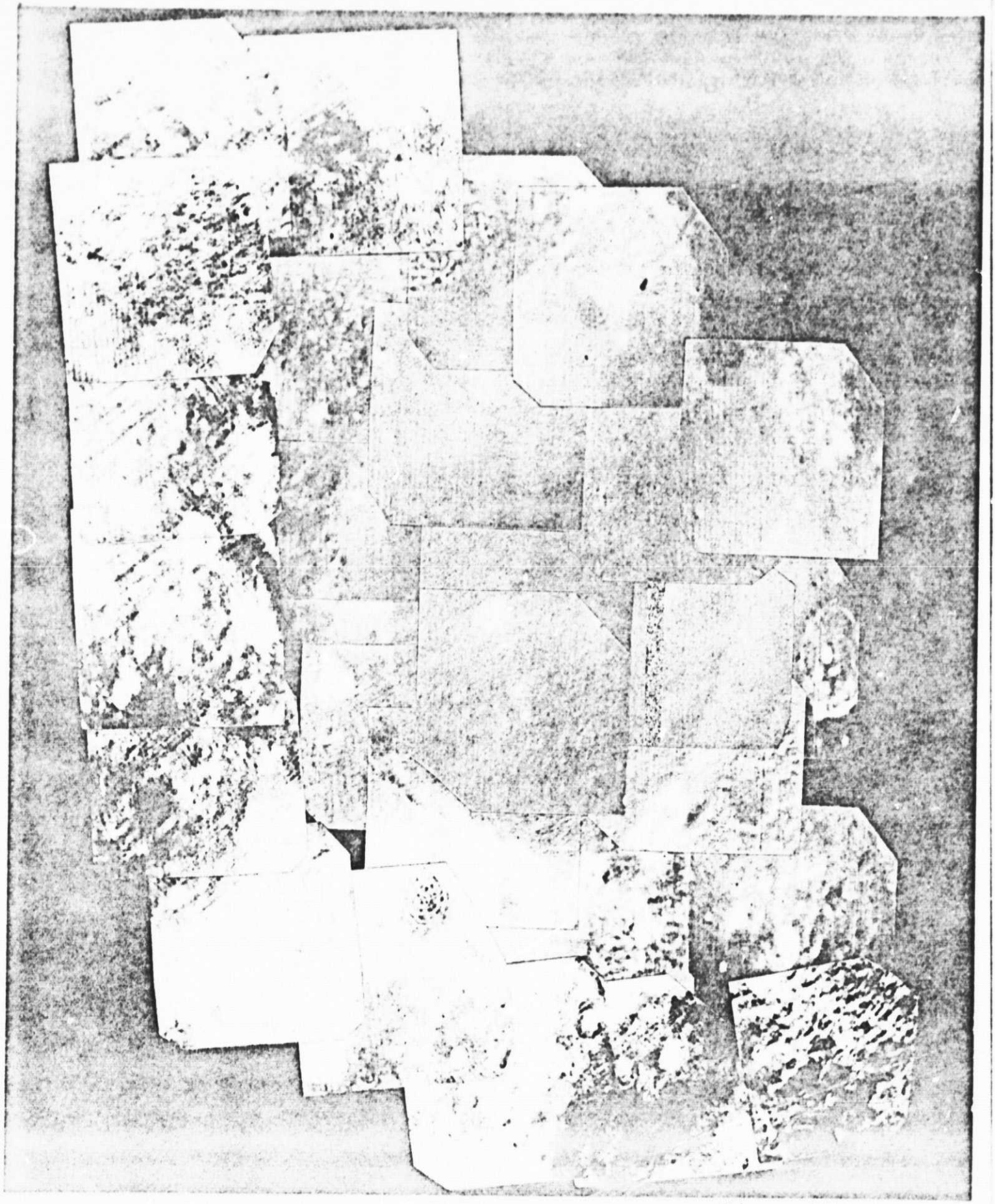

Figure 15b

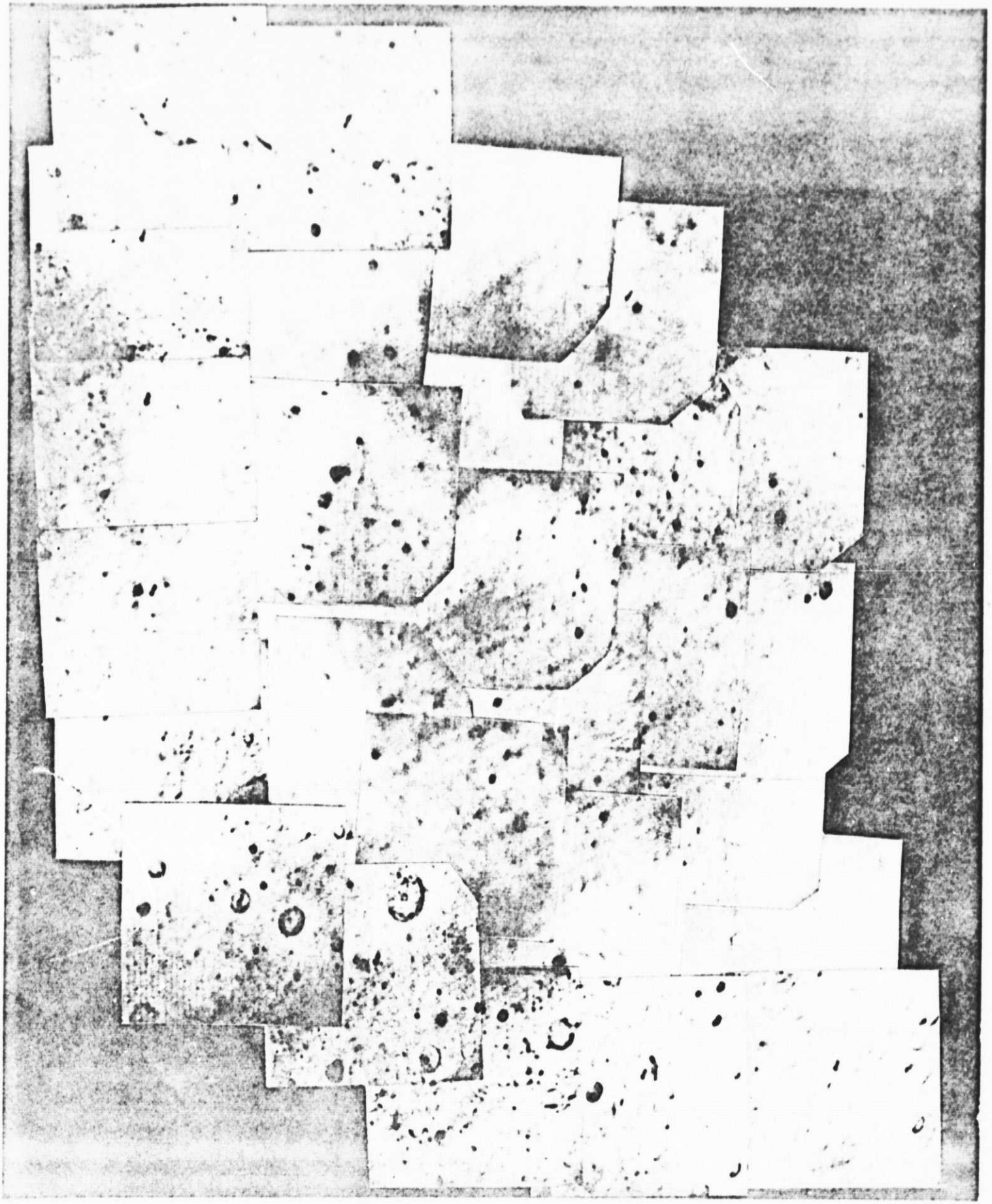

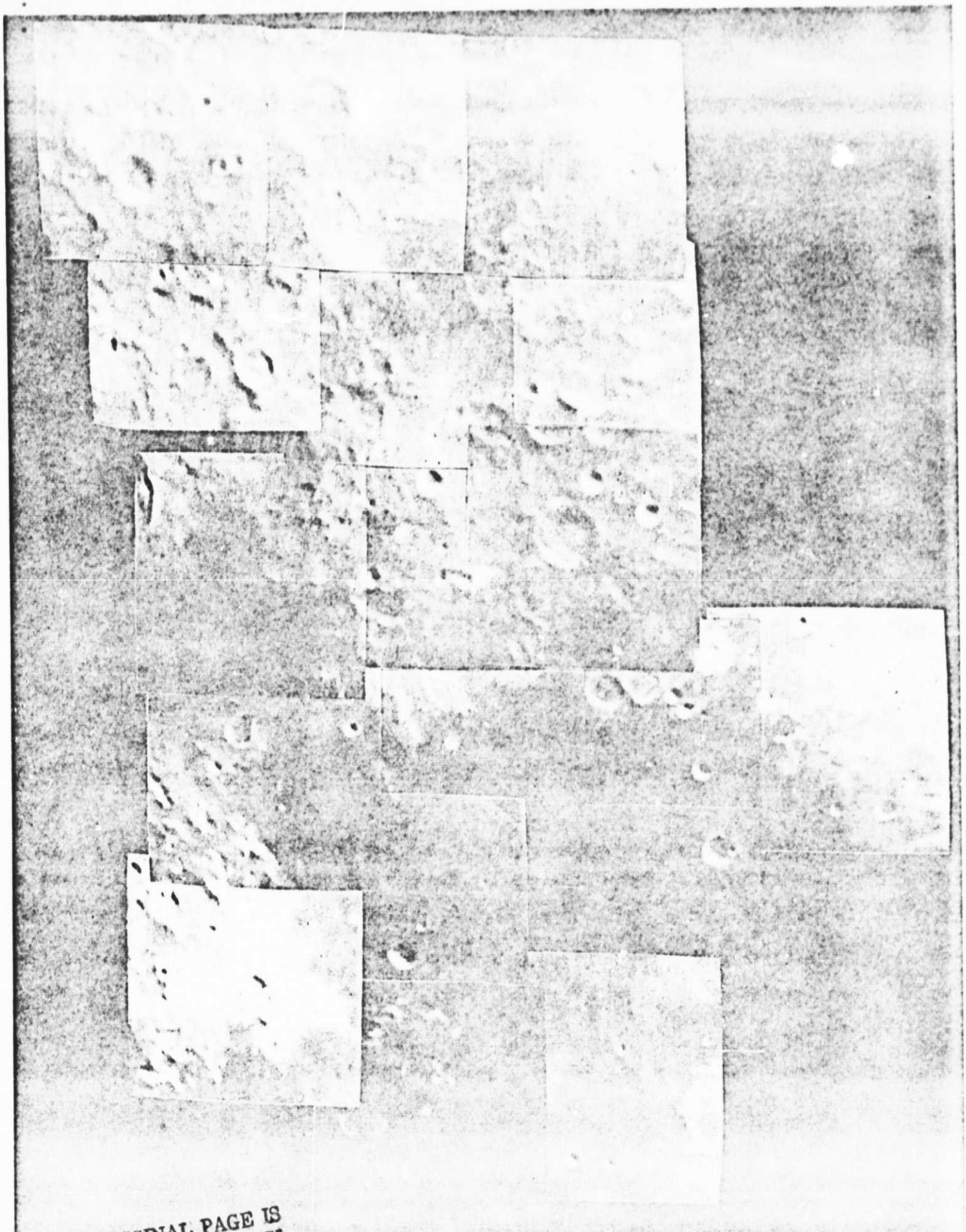

Figure 16c

Figure 17

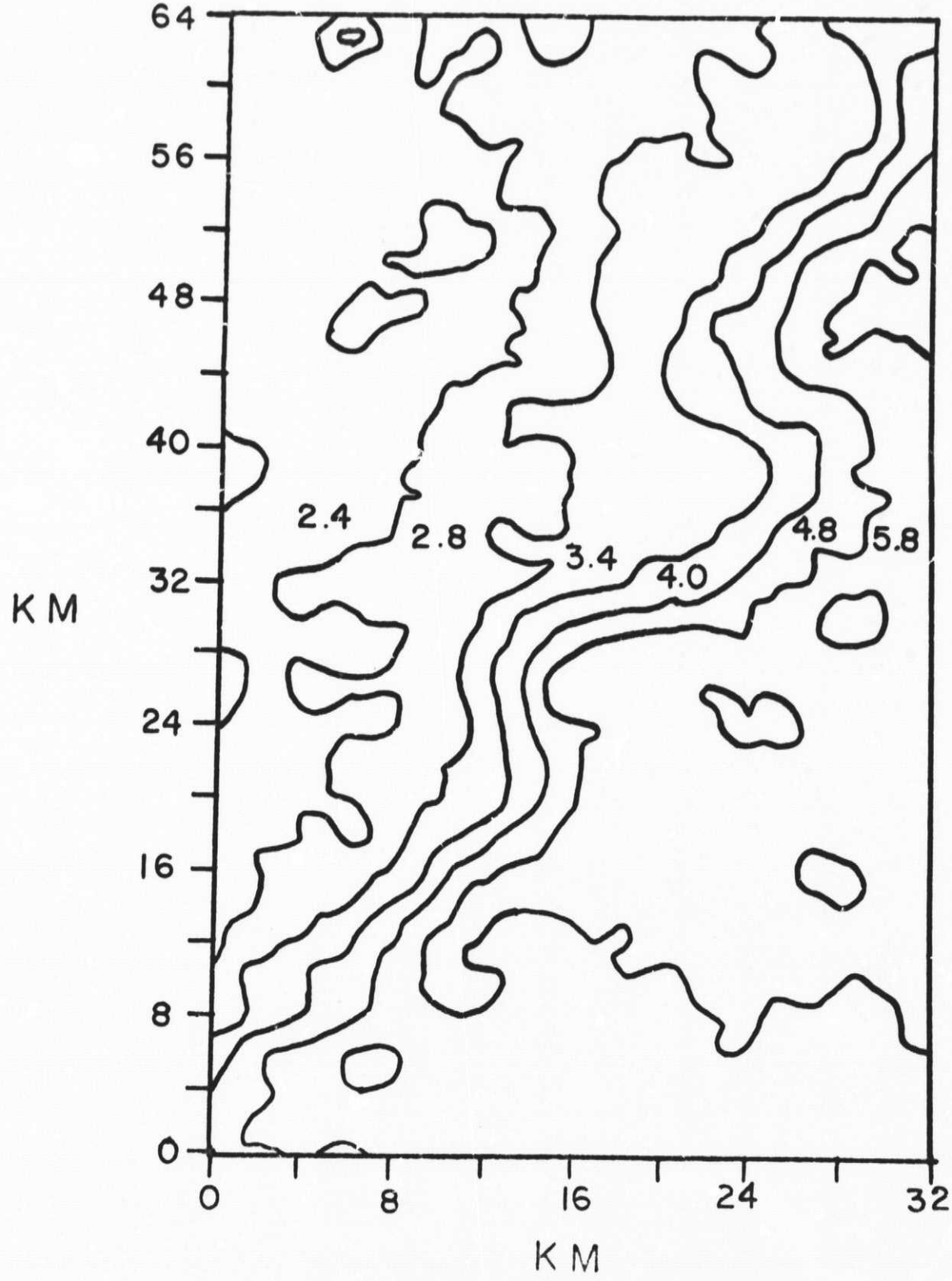

Figure 18

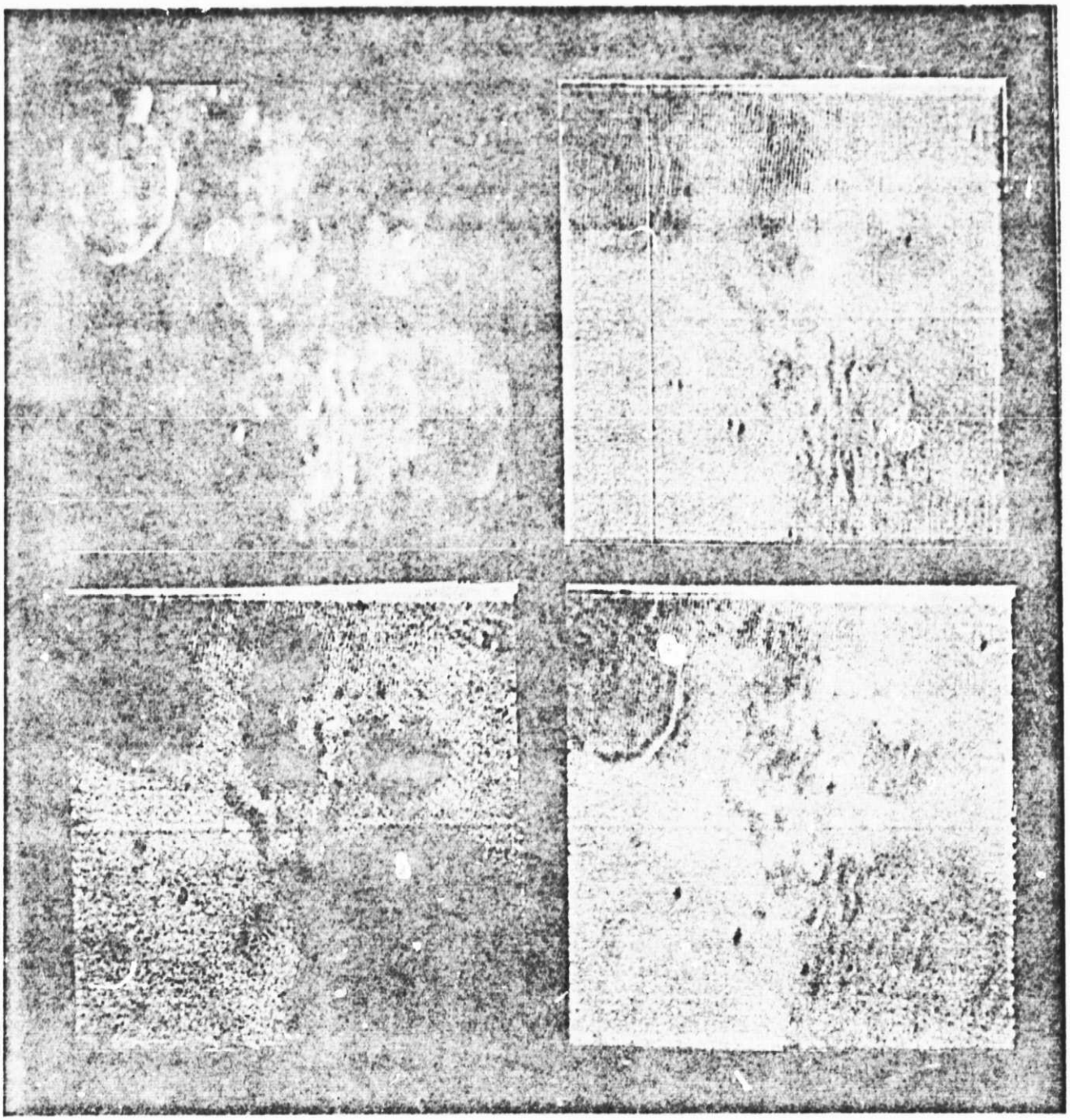

Figure 19

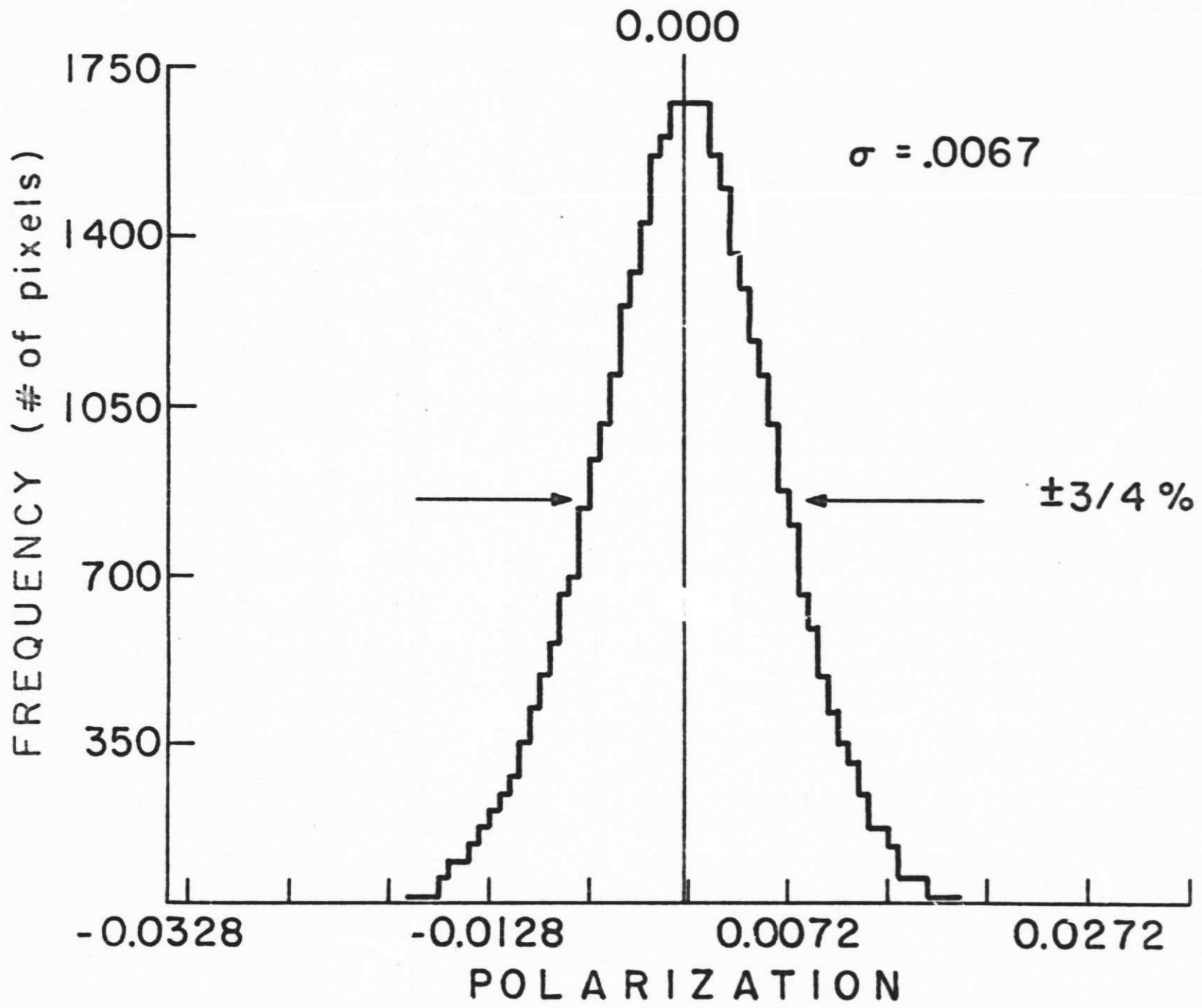
0.000
1750
1400
1050
700
350
FREQUENCY (# of pixels)
σ = .0067
±3/4 %
-0.0328
-0.0128
0.0072
0.0272
POLARIZATION

Figure 20